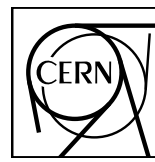


EUROPEAN ORGANIZATION FOR NUCLEAR RESEARCH



Apparatus for Meson and Baryon
Experimental Research



CERN-SPSC-2023-024

SPSC-SR-333

August 24, 2023

AMBER Status Report 2023

The AMBER Collaboration

Abstract

The report reviews the activities and the achievements of the Collaboration towards the current date. Covered items are the first completed data taking for antiproton production cross-section measurements, ongoing analysis and plans for 2024 running time; collected data so far and the preparations for the future runs for the measurements of the Proton Charge-Radius; preparations for the meson structure measurements by using Drell-Yan process, first results of Cherenkov detectors (CEDAR's) test with high hadron beam intensity.



Contents

1	Introduction	3
2	Antiproton Production Cross-Section Measurements	3
2.1	The November 2022 Test Run	3
2.2	Preparation to 2023 antiproton cross section run	3
2.2.1	RICH beam-pipe removal	3
2.2.2	CEDAR preparation	4
2.2.3	Target preparation	7
2.2.4	Detectors preparation	8
2.2.5	Trigger preparation	9
2.3	Summary of the 2023 physics run	10
2.4	Status of the analysis of the 2023 physics run	11
2.5	Proposal for the 2024 run: Measurement of \bar{p} production cross-section in proton-proton collisions	12
3	Proton Charge-Radius Measurement	16
3.1	Results from the 2021 Pilot Run	16
3.2	Ongoing Activities and Plans for 2023	19
3.2.1	Status and Plans for the 2023 Beam Time	19
3.3	Plans for 2024/2025	22
4	Meson structure measurement by using Drell-Yan process	23
4.1	First results of the Cherenkov detectors (CEDAR's) test with high intensity hadron beam. . .	23
5	Hardware	26
5.1	TPC and Gas System	26
5.1.1	Preparation of the IKAR TPC for 2023	26
5.1.2	Preparation of the New TPC	27
5.2	Unified Tracking Station	29
5.2.1	Beam Test in 2022/2023	29
5.2.2	Scintillating Fiber Hodoscope (SFH)	31
5.2.3	Silicon Pixel Detector (SPD)	31
5.3	New Large Area Micromegas detectors	35
5.4	DAQ	36
5.4.1	HLT Structure	37
5.4.2	HLT Infrastructure @ Batch Service	37

5.4.3 DAQ Architecture for 2023 Run	38
6 Publications, presentations to conferences and collaboration matters	40
7 References	41

1 Introduction

The report describes first results of the antiproton production cross-sections measurement, and the status of the preparations for the proton charge-radius measurement and the meson structure measurement via Drell-Yan process, as well as the respective developments in hardware and organisation. The different physics cases are split into separate sections. Additional hardware-related information can be found in the dedicated hardware part of the document. This document is takes into account information presented in the previous SPSC report of 2022 [1]. The given information covers the time between the release of the last report and the date of this report.

2 Antiproton Production Cross-Section Measurements

In this section we present an update on the Antiproton Production Cross-Section Measurements, in particular regarding the preparation of the 2023 run and the data taking performed in May and June. The measurement of the double differential antiproton production cross section from the proton-He interactions is possible thanks to the excellent track reconstruction of the AMBER spectrometer and particle identification by RICH-1.

2.1 The November 2022 Test Run

The test run announced in the previous SPSC report [1] took place from November 9th to November 14th 2022, using the polarised LiD COMPASS target and a positive hadron beam with an intensity of about $5 \cdot 10^5$ p/s. The different target introduced some limits mostly because when compared to the liquid-He the LiD target is more dense by a factor 3. The larger density was compensated by pre-scaling the trigger. The experiment was operated with the minimum-bias trigger then used also for the Run 2023, which includes: beam trigger and veto, to ensure that the particle reaches the experiment within the geometrical target acceptance; beam killer 1 (BK1) and 2 (BK2) installed downstream of the SM2 magnet to remove the non-interacting beam particles from the trigger. Data were collected at four different beam momenta between 60 and 250 GeV and consequently with different spectrometer magnets (SM1 and SM2) current settings. The position of the beam killers was optimised performing a scan of the counting rates as a function of the position along x - and y -axis for each configuration shown in Tab. 1.

Table 1: The different configurations tested in the November 2022 Test Run are shown in this table.

Beam momentum (GeV/c)	SM1 (A)	SM2 (A)	BK1 (x, y) (mm)	BK2 (x, y) (mm)
60	936	0	(102, 6.0)	(180, 5)
60	936	1500	(103, 7.5)	(139, 5)
60	2500	0	(45, 7.7)	(59, 5)
100	1562	2500	(107, 6.0)	(188, 5)
190	2500	4800	(85, 0.0)	(155, 0)
250	2500	4800	(67, 11.0)	(118, 11)

Monte Carlo simulations have been run to study the Spectrometer performance in the different tested configurations. In Fig. 1 the tracking reconstruction efficiency for all the four beam momenta is presented. The results obtained for the three configurations at 60 GeV are very similar and only the one for SM1 current 2500 A and SM2 off is shown. No significant dependency from the reconstructed track momentum for any of the beam energy is observable.

2.2 Preparation to 2023 antiproton cross section run

2.2.1 RICH beam-pipe removal

The RICH acceptance is a characteristic feature that defines the phase space where the particle ID is possible, i.e. the antiproton momentum and directions that can be explored. The RICH-1 detector is a very large ($3.5 \times$

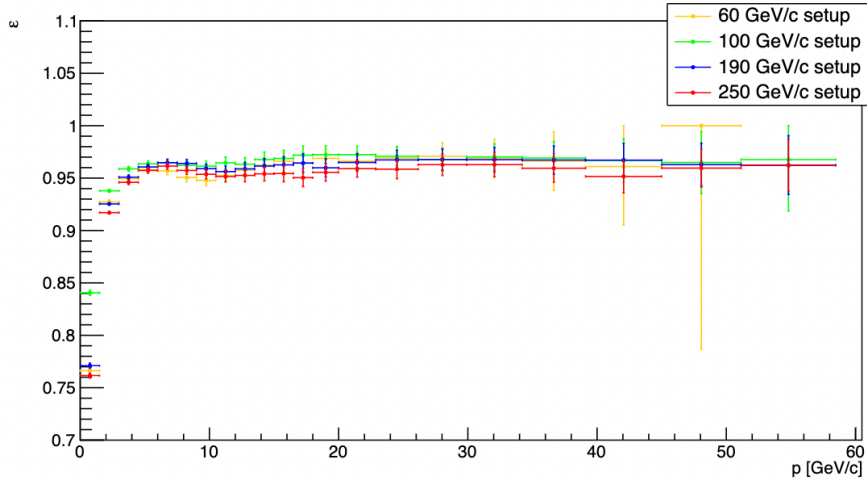


Fig. 1: Tracking efficiency as a function of the particle momentum for four beam momenta configurations of the test run. At 60 GeV only the configuration with SM1 current 2500 A and SM2 off is shown.

$4 \times 3.5\text{m}^3$) volume filled with C_4F_{10} ; when a charged particle traverses this gas with $\beta\gamma > \sim 18$ a cone of Cerenkov light is generated. The aperture angle (θ) of the light cone is proportional to the gas refraction index (η) and the particle relativistic velocity (β) through the very well known relation:

$$\cos \theta = \frac{1}{\eta \beta}$$

In the standard configuration of the spectrometer setup RICH-1 is equipped with a so called beam-pipe, i.e. a cylindrical bag made of aluminised Mylar with a diameter of 10 cm and length corresponding the whole RICH length, filled with He gas. The axis of this cylinder is aligned with the beam direction. The purpose of this cylinder is to prevent Cerenkov light production by beam particles. This beam-pipe became necessary for the high intensity muon beam to prevent pile-up which would degrade the RICH-1 performance. In the case of a low intensity proton beam such pile-up is not an issue. On the contrary the presence of the beam-pipe prevents the identification of the antiprotons at a small angle with respect to the beam and also reduces the efficiency for those antiprotons whose Cerenkov cone crosses only partially the beam-pipe. A detailed MC study shows the effect as summarised in Fig. 2.

The presence of the RICH-1 beam pipe would prevent the identification of antiprotons with pseudo-rapidity larger than ~ 5.5 and reduces the efficiency for those antiprotons with pseudo-rapidity in the range from 4 to 5.5. Therefore, the RICH-1 beam-pipe was removed. Figure 3, produced with a MC simulation, shows the Cerenkov rings recovered after the beam pipe removal.

2.2.2 CEDAR preparation

For a proper measurement of the antiproton production cross section in p-He interactions, in principle a clean proton beam is needed. However, the secondary hadron beam from the SPS M2 beam line contains a composition of positively charged hadrons; mostly pions, kaons and protons. The relative composition depends primarily on the selected beam momentum, with a pion dominated beam at lower momenta and a proton dominated beam at higher ones. To properly identify the protons in the mixed hadron beam we use a special Cerenkov threshold detector called CEDAR. CEDARs are available at CERN since the 80s and they consist of a ~ 4.5 m gas filled cylinder, with a set of mirrors at the end which collect the Cerenkov radiation and form a Cerenkov ring. The ring is focused on a plane where 8 multi-anode PMTs, placed evenly along the circumference, can detect the Cerenkov light. A circular diaphragm system, lets the PMTs be sensitive only to Cerenkov rings of a selected narrow radius range. Once the CEDAR detector is properly aligned with respect to the beam direction, the Cerenkov ring correctly hits all of them. Ideally a particle crossing the CEDAR with a speed within the selected range should produce an 8-fold PMT coincidence. A coincidence of less than 8 PMTs should occur

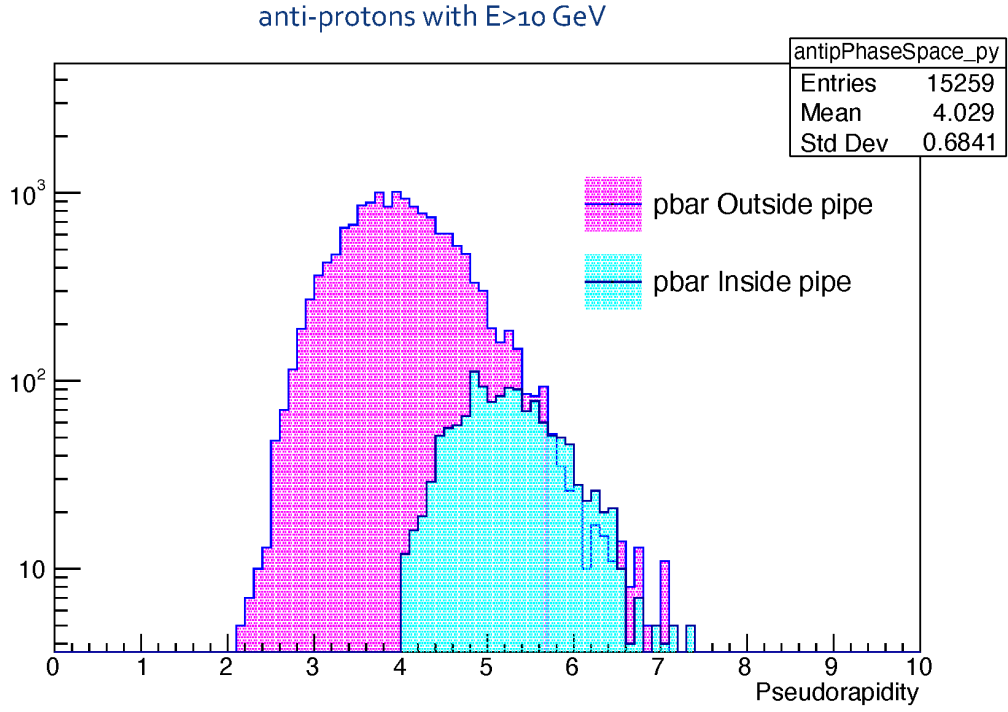


Fig. 2: Prompt antiproton from p-He interaction pseudo-rapidity distributions. The magenta distribution corresponds to antiprotons not affected by the RICH-1 beam pipe, the cyan distribution those that instead are affected by the RICH-1 beam pipe.

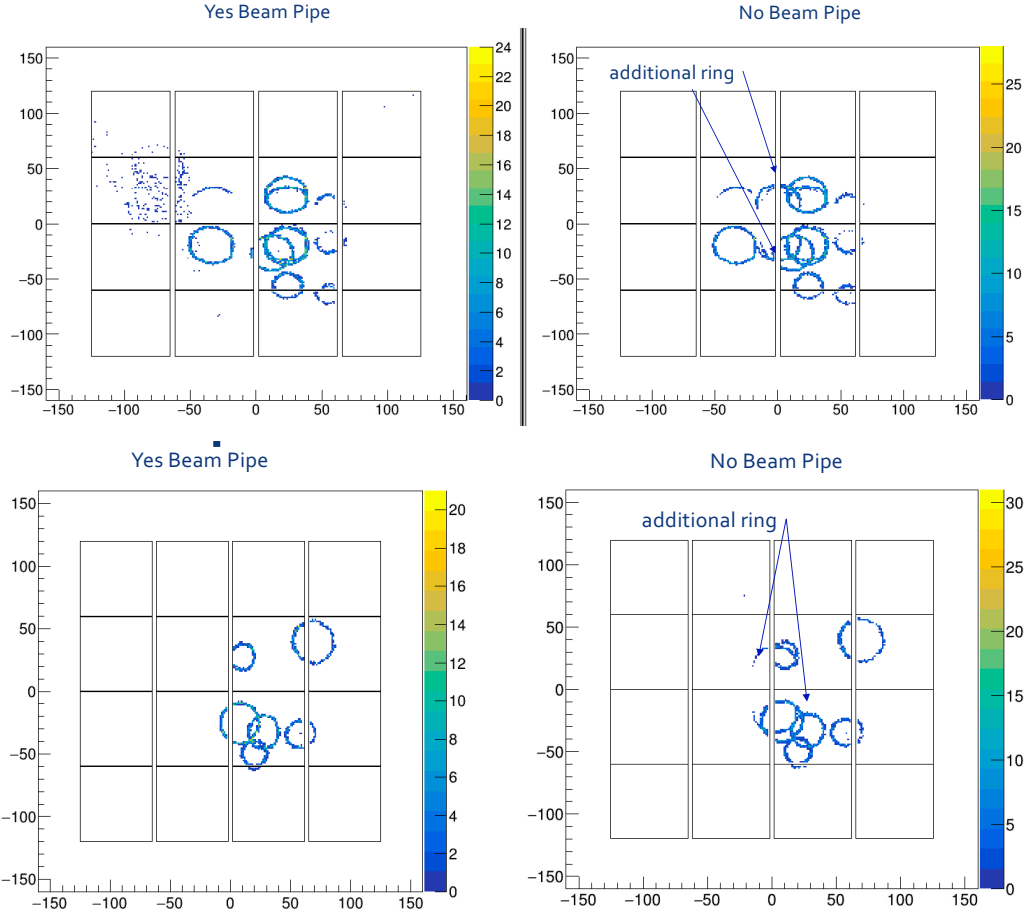


Fig. 3: Examples of the effect of the RICH-1 beam pipe on the detected Cerenkov rings.

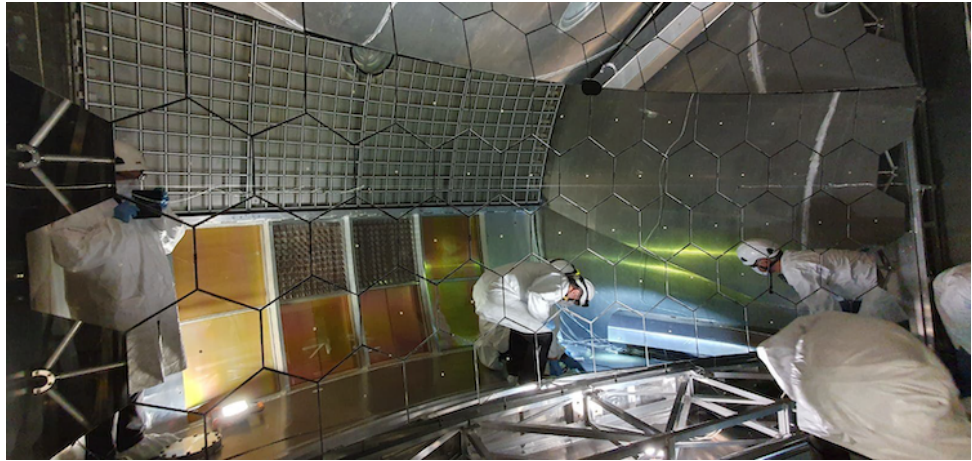


Fig. 4: A picture taken inside the RICH-1 vessel during the beam pipe removal operation.

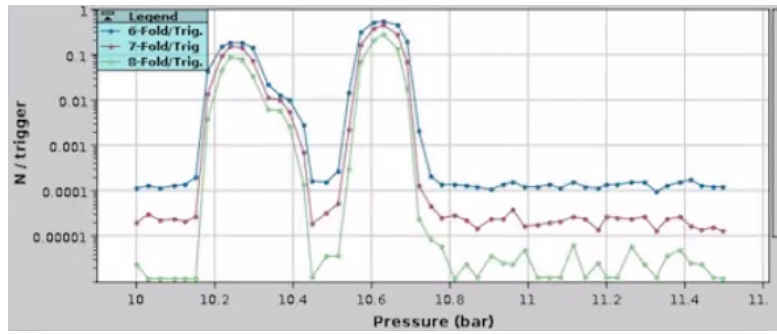


Fig. 5: CEDAR-N 1, n-fold PMT coincidence versus the gas pressure with 190 GeV/c hadron beam; left to right it is easy to identify the pion, kaon and proton peak.

either because of not perfect PMT efficiency or because of random noise. The velocity range for the CEDAR signal can be set either changing the gas pressure, and hence the refraction index, or adjusting the diaphragm aperture. Figure 5 shows the n -fold PMT coincidence versus the gas pressure with 190 GeV/c hadron beam. It is very easy to identify, left to right, the peaks from pions, kaons, and protons. It is also very evident how the proton peak is well isolated, confirming that they can be selected very efficiently and with a very high purity.

After several meetings and discussions with the CERN M2 beam-line responsible, it resulted that it was possible to install two so-called CEDAR-N in sequence, each one with its thermal enclosure and a forced air system that keeps the CEDAR gas temperature constant. The use of two CEDAR detectors allows to improve particle identification purity. Over the winter shutdown the CERN M2 beamline experts installed and pre-aligned the two CEDAR-N, upstream with respect the spectrometer. According to the documentation [2] the CEDAR-N lower threshold was not enough to identify protons with the hadron beam at 60 GeV/c momentum. As contingency plan, the CERN M2 beam line experts offered to use a different type of threshold Cerenkov counters, used in pair to set the desired velocity range. During the commissioning, tests were performed with a 60 GeV/c hadron beam, and it was observed that CEDAR-Ns were still very efficient in identifying protons in the beam. During the data taking, a CEDAR tuning procedure was completed each time a new beam energy was set. The procedure includes first an optimisation of the two CEDARs alignment with respect to the beam direction, and then an adjustment of the gas pressure and the diaphragm aperture to make the CEDAR produce PMT coincidence only when a proton passes.

Figure 6 relates to the 190 GeV/c hadron beam. For each beam trigger generated by the spectrometer, the number of coincident PMT hits is available for CEDAR 1 and CEDAR 2. In this figure one can identify three different zones. The first one corresponds to 0 PMTs hit in either CEDAR. The second zone corresponds to a coincidence larger than or equal 6 PMTs in CEDAR1 and 7 or 8 PMT hits in CEDAR2. The third zone corresponds to the remaining cells characterised by a low occurrence (deep blue color). The second zone, whose asymmetrical size is due to a known slightly smaller PMT efficiency on CEDAR1, corresponds to identified

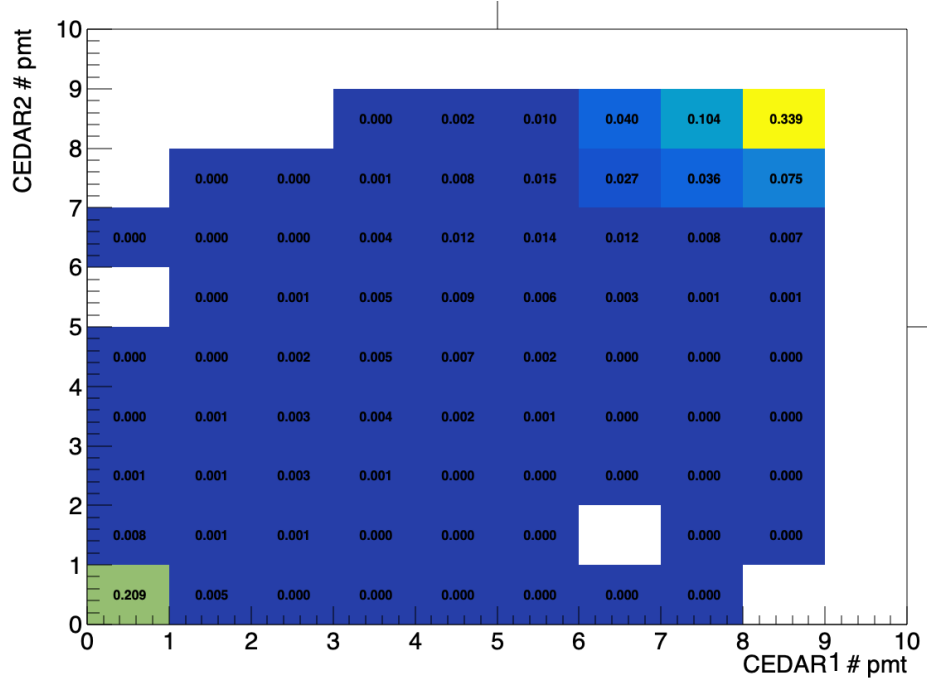


Fig. 6: Table of the CEDAR2 vs CEDAR1 n -fold coincidence for each beam trigger generated by the spectrometer.

protons. It is interesting to observe that the second zone is well distinguished from the random coincidences of the third zone, and that the second zone counts overall for $\sim 63\%$ which match the expected proton fraction in the 190 GeV/c hadron beam.

In the last part of the data taking, specific runs have been made to measure the CEDAR capability to select a pure proton sample from the mixed hadron beam. This way, the probability of a false positive for a single CEDAR detector has been measured.

We performed the first measurement with the 250 GeV/c hadron beam. We set the CEDAR1 to produce signal for pion/kaon and we requested a 8-fold PMT coincidence, selecting then a quite pure pion/kaon sample. We then set CEDAR2 to produce signal for protons instead (7 or 8 fold coincidence), and we counted how many times it fired. Out of 15415 events of pure pion/kaons, according to CEDAR1, only 2 events have been identified as protons by CEDAR2.

Inverting the roles of the two CEDARs, out of 32407 events recognised as pion/kaon by CEDAR2 (8 fold coincidence) only 3 events have been identified by CEDAR1 as protons (6, 7 or 8 fold coincidence). This means a proton identification false positive rate of at most $1.3 \cdot 10^{-4}$ for CEDAR1 and $0.9 \cdot 10^{-4}$ for CEDAR2. The combined false positive rate of the two CEDARs is measured to $1.2 \cdot 10^{-8}$. Even in the most difficult case of the 60 GeV/c hadron beam where the expected beam proton fraction of the order of 20%[3], the two CEDARs rejection power guarantees a practically pure proton sample to study the p-He interactions.

2.2.3 Target preparation

The new liquid ^4He target has been realised starting from an existing apparatus used for the COMPASS polarised LiD target in 2022 (see figure 8). In fact the dilution refrigerator is well suited also for the liquid ^4He target. The three target cells and the ^6LiD material of the SIDIS COMPASS polarised target have been removed and the mixing chamber has been filled with liquid ^4He for a total length of 140 cm and a diameter of 7 cm. The ^4He is maintained at a temperature of about 1 K by the refrigerating system, that makes the liquid super fluidity. The solenoid and dipole magnets and the microwave cavity, that were used for dynamic nuclear polarisation in COMPASS are kept in place for thermal shielding. The target system started cooling from the middle of March with supports of TE- CRG and EP-DT groups. All in all, the target preparation, commissioning and operation

was very smooth during this year run.

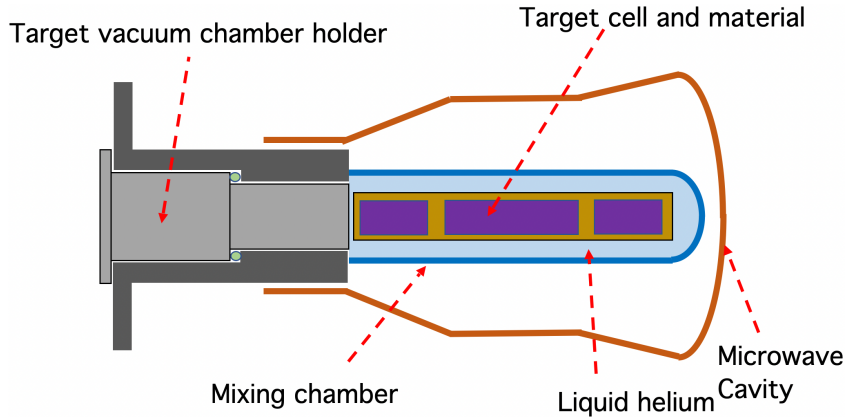


Fig. 7: An illustrative scheme of the former COMPASS polarised target, now used as He-Target. A more complete and detailed view of the system is shown in figure 7.

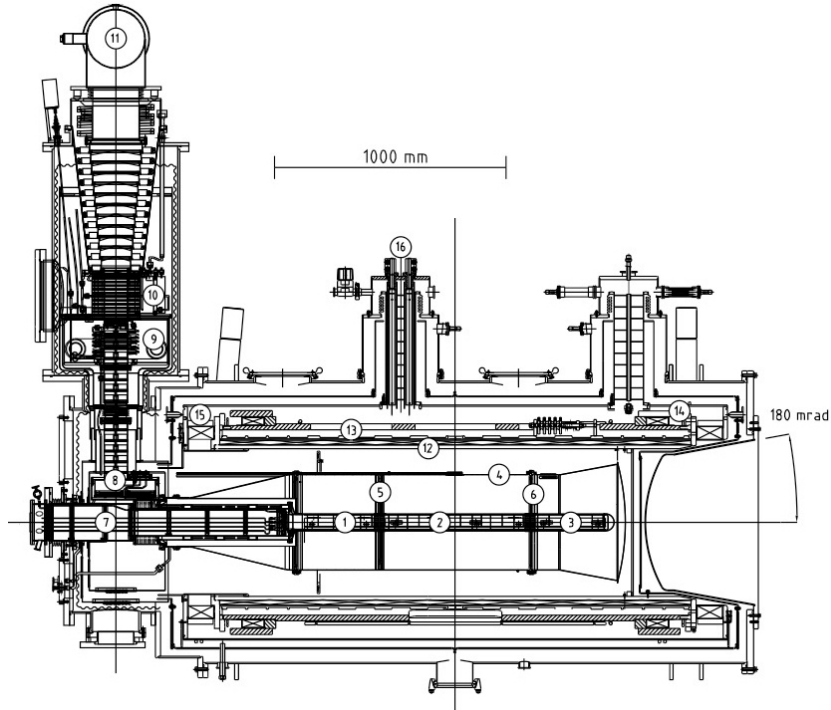


Fig. 8: SideView of the COMPASS polarised target: (1) upstream target cell, (2) middle target cell, (3) downstream target cell, (4) microwave cavity, (5) upstream microwave stopper, (6) downstream microwave stopper, (7) target holder, (8) still or ^3He evaporator, (9) ^4He evaporator, (10) ^4He liquid/gas separator, (11) ^3He pumping port, (12) solenoid magnet, (13) correction coils, (14) dipole coil, (15) solenoid end compensation coil, (16) magnet current leads.

2.2.4 Detectors preparation

During the winter shutdown, some maintenance and refurbishment work has been done on the detectors. In particular, for the Multi Wire Proportional Chambers (MWPCs) the station PB06 was refurbished with the replacement of one front aluminised mylar window with a spare one. In fact the breaking of the metallised part of the mylar foil was at risk of increasing the noise level and electrical instabilities, as observed in the past recent years for other MWPCs which have been then refurbished.

A intensive and systematic exchange and study of the front-end cards for the RichWall lead to a solution which enabled us to operate

The beam target setup which had to be removed for unloading the polarized target at the end of 2022 was reinstalled including three scifi stations, 5 fast plastic scintillator veto hodoscopes and three cold silicon stations.

Since the malfunction of Pixel Gem 3 in 2022 could not be debugged in situ, a spare pixel gem was used to successfully exchange the broken detector during the commissioning phase.

The two electromagnetic calorimeters were maintained and calibrated in two steps with electron beam. Improvements in the trigger system and beamline configuration tripled flux which could be used and therefore shortened the time needed for the calibration campaign.

2.2.5 Trigger preparation

The principle of the minimal bias trigger system was tested during the 2022 test run and further optimized afterwards. For the 2023 measurement the beam trigger (BT) signal was composed out of a coincidence of two orthogonal planes of SciFi detectors in the beam telescope which are placed 5m apart in front of the target with an acceptance of $4 \times 4 \text{ cm}^2$. This beam trigger covered the central part of the mixing chamber of the polarized target as shown in Fig. 14 top right. A veto (V) system consisting of seven beam halo vetos in front of the target excluded events with signals outside the target acceptance and pile-up events including a beam halo particle. The trigger system was completed by two non-interaction vetos behind SM2 and in front of ECAL2. These so called beam killer (BK) scintillator elements consist out of an circular plastic scintillator disc of 2 mm thickness placed in an air light guide and readout by a PMT. This setup was chosen to minimize the material in the hadron beam. The beamkiller were placed on the bending beam axis behind the spectrometer magnets and the diameter of the scintillator disc was chosen depending on the beam energies and the expected spread of non interacting particles at the given z positions. Both beam killer elements were put in coincidence. Depending on the beam energy also the position of beam killer discs had to be varied. To allow remote position two x-y tables were constructed as shown in Fig. 9.

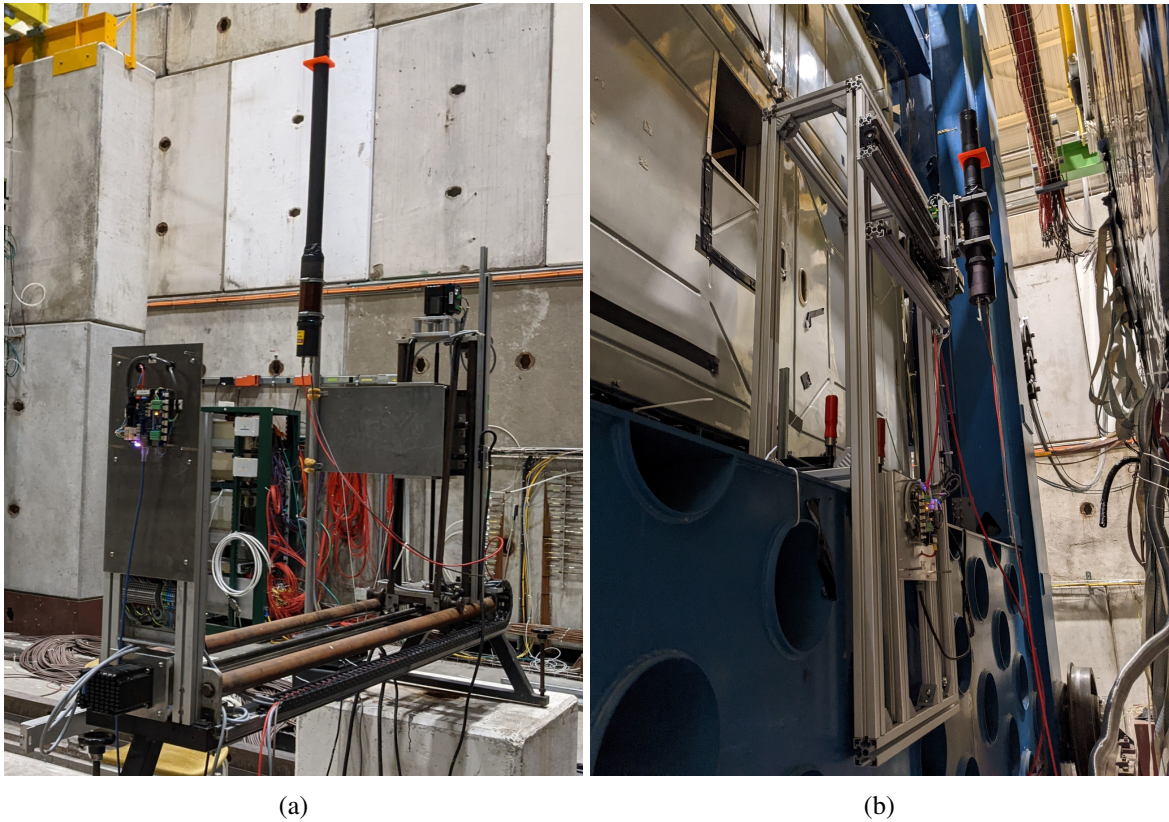


Fig. 9: Figure (a) shows the x-y table of BK1 behind the first spectrometer magnet. Figure (b): Table of radio-protection designated areas and their respective limits.

Table 2: Conducted measurements during the 2023 physics run.

Beam momentum (GeV/c)	Collision energy ($\sqrt{s_{\text{NN}}}$) (GeV)	Start Date	End Date	Number of spills
60	10.7	24.05	30.05	37000
80	12.3	17.06	25.06	13400
100	13.8	01.06	11.06	13700
160	17.3	14.06	17.06	8500
190	18.9	19.05	24.05	11000
250	21.7	11.06	14.06	7300

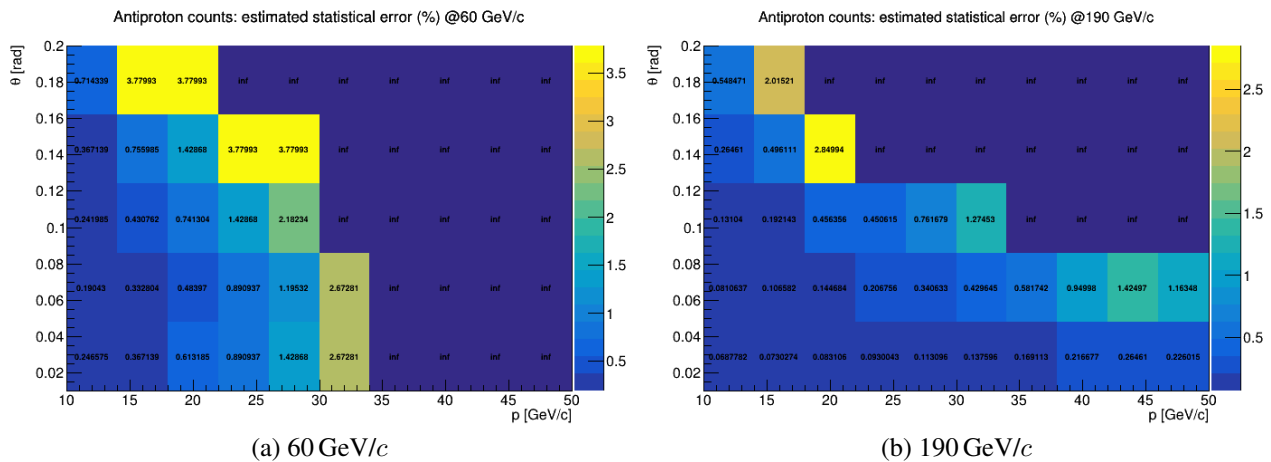


Fig. 10: Exemplary statistical precision of the recorded datasets at 60 GeV/c and 190 GeV/c.

This allowed to position the discs remotely after beam tuning for the different beam energies. The three trigger components were used to generate the physics trigger: BT x !V x !BK. The different subcomponents were also inserted to the prescaler of the DAQ to allow studies of the different trigger components and response of the detector systems.

2.3 Summary of the 2023 physics run

The 2023 data-taking period for the antiproton production cross-section measurement in proton-helium collisions started on 28 April. During commissioning several operations were carried out, of which the most time consuming was the calorimeters calibration. The calibration of ECAL1 and ECAL2 was performed using a 40 GeV/c electron beam crossing the spectrometer with empty target. The calorimeters are moved perpendicular to the beam to cover every module. Having the calorimeters working is very important in order to possibly extract from data the production cross section of $p + {}^4 \text{He} \rightarrow \pi^0 + X \rightarrow \gamma + X$ (See Sec. 2.5).

After completion of detector commissioning, physics data taking started on 19th May. In total, data at six different beam momenta were recorded. An overview of the different beam momenta, the corresponding collision energy, the start and end dates, and an estimate of the collected number of spills are summarised in Tab. 2.

Besides collisions at 60 GeV/c, 100 GeV/c, 190 GeV/c, and 250 GeV/c, which were tested during the 2022 test run (see Sec. 2.1), additional collisions at 80 GeV/c and 160 GeV/c were taken. The recorded data at those beam momenta complement existing measurements of antiproton production in proton-proton and proton-carbon collisions taken by the NA61 and NA49 collaborations [4–6] and allow further studies of the scaling of the antiproton production cross-section from proton-proton to proton-nuclei collisions. The number of recorded spills for each collision energy was chosen so that the statistical precision in most part of the antiproton phase-space covered by the experiment is better than 1 %. Exemplary, Fig. 10 shows the estimate for the reached statistical precision of the recorded data sets at 60 GeV/c and 190 GeV/c.

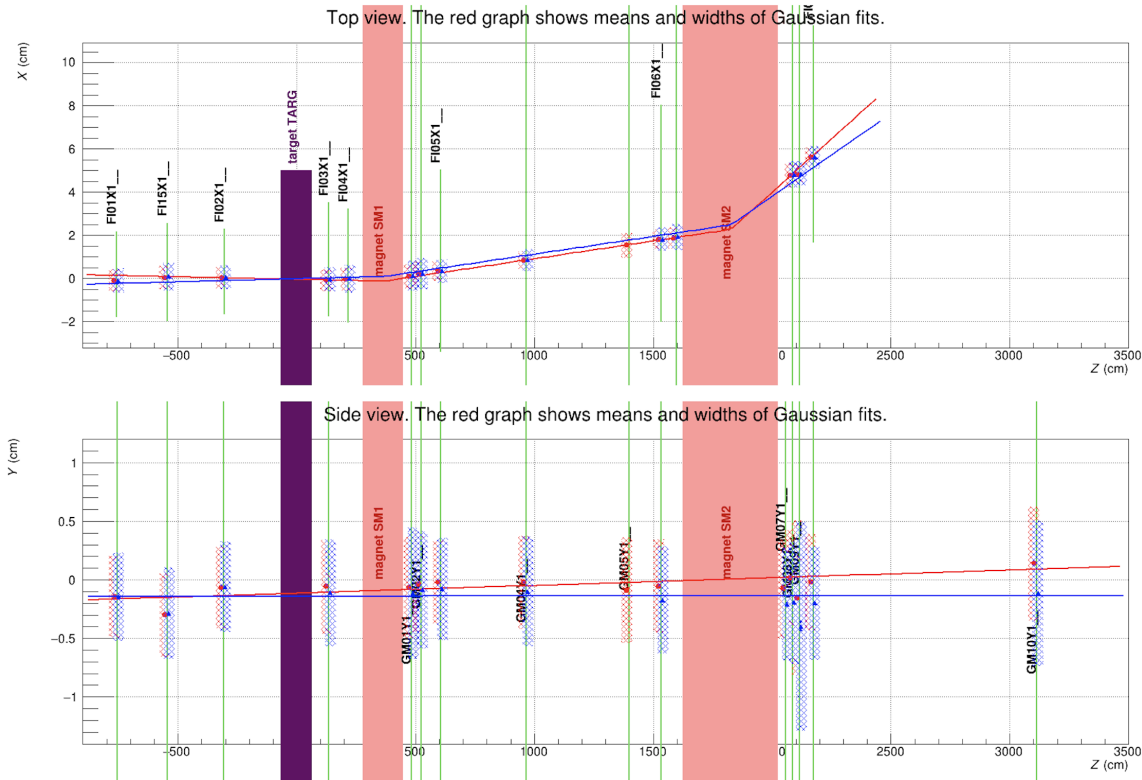


Fig. 11: Measured beam trajectory through the AMBER spectrometer for two different beam momenta. In red, 160 GeV/ c is shown, and in blue, 190 GeV/ c .

To minimise variations of systematic uncertainties between the different collision energies, the traversing path through the spectrometer at all beam momenta were tuned to follow as closely as possible the same trajectory. This was achieved by fine-tuning the beam-line magnets and the spectrometer magnets SM1 and SM2 for each beam momentum. In Fig. 11, exemplary the measured beam trajectories for 160 GeV/ c and 190 GeV/ c through the spectrometer are shown.

For further studies of systematic uncertainties, additional runs were performed for each beam momentum: Alignment runs, trigger-efficiency runs, and empty-target runs. The alignment runs will be used to check the alignment of the detectors of the spectrometer and identify potential movements of the setup during the data-taking period. The alignment runs were performed using a broad 160 GeV/ c muon beam and data were taken with the spectrometer magnets switched off and on. For the trigger-efficiency runs, different combinations of the different trigger conditions applied to the physics runs (beam trigger, beam killer, veto) were used. By comparing the rates of the different combinations, the efficiencies of the different conditions can be extracted. After the recording of the physics-run data with the liquid helium target, additional runs have been recorded for each beam momentum in an empty-target configuration, in which the helium from the target has been evacuated. These runs shall serve to reduce the background from scattering events on the target material other than helium.

2.4 Status of the analysis of the 2023 physics run

The recorded raw data from the 2023 antiproton production measurement campaign is around 460 TB, which has been stored on CTA. It was kindly agreed with the COMPASS collaboration to store the data within the COMPASS quota to minimise overhead work and computing resources during the preparation and execution of the beam time for AMBER. As a first step, we started to analyse the recorded data from the first period (W01). Specifically, the spectrometer's first alignment is ongoing to allow efficient track reconstruction for the following analysis steps. The alignment procedure is based on the method developed by the COMPASS collaboration, and the current preliminary results have been discussed with experts from COMPASS and AMBER in

joint analysis meetings to optimise the information flow between both collaborations. The alignment procedure using alignment run data from W01 is progressing well; a few iterations have already been performed making corrections based on the available detector survey information and updated detector calibrations. The difference of the hit on the detector and the position of the track reconstructed at the detector itself is called residual. The alignment procedure consists mainly in centering the residual distribution around 0 and plotting residual distribution along parallel and perpendicular coordinates with respect to the sensitive elements of the detectors (e.g. wires). As an example, in Fig. 12 the residuals distribution on the y axis vs the coordinate perpendicular to the silicon strip is plotted after the alignment procedure for the silicon station 2 U and V planes. The almost perfect horizontal fit line means that the stations are not tilted and the intercept shows the very good centering of the detector.

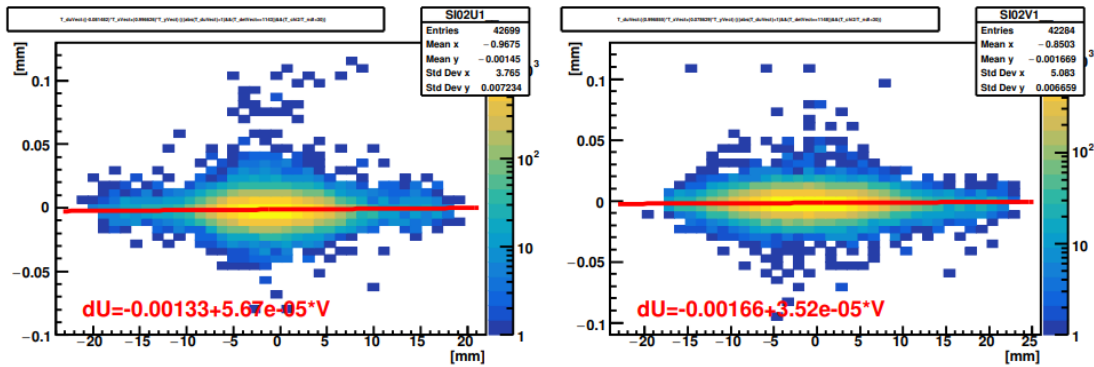


Fig. 12: Residuals distribution of the X,Y track coordinates obtained after the application of the alignment procedure on the Silicon station 2 U and V planes.

Alignment quality is also being checked looking at the detector pseudo-efficiencies (see Fig. 13). The pseudo-efficiencies are evaluated on a period by period basis to check stability of detectors but also serve as an important input to check tensions between neighbouring detectors in the tracking algorithm due to relative misalignment. Furthermore, they serve as an important input for the MC simulations to best describe the spectrometer conditions during the data-taking.

After a first round of alignment is completed, one can start looking at the performance of the reconstructing algorithm and in general at the kinematics of the events. For instance Fig. 14 shows primary vertex position distribution, in which our cylindrical He target is clearly evident with dimension of 3.6 cm in radius and 140 cm in length. This is a very clear picture showing good vertex reconstruction capabilities that are crucial in order to distinguish prompt from non-prompt antiproton production.

The (anti-)hyperon production is also of interest in our analysis first of all to disentangle the secondary contribution of antiprotons coming from decays and secondly because the so-called V0s are used to estimate the RICH-1 PID efficiency.

The PID relies on the Cerenkov light produced in the RICH-1 as discussed in previous sections. The Cerenkov cone angle is a function of the velocity of the particle and hence of its momentum. In Fig. 15 a plot from fresh data is showing the Cerenkov angle versus the particle momentum. One can identify the characteristic bands representing electrons, pions, kaons and protons (both positive and negative). One can exploit for instance the decay channel $\bar{\Lambda} \rightarrow \bar{p} + \pi^+$ to obtain clean samples and assess at the performances of the RICH-1 detector in the antiprotons identification (see Tab. 3).

A selection of these secondary vertices from the new collected data is shown in the Armenteros-Podolanski plot in Fig. 16.

2.5 Proposal for the 2024 run: Measurement of \bar{p} production cross-section in proton-proton collisions

The experimental accuracy of the order of a few percent achieved by AMS-02 on the cosmic-ray \bar{p} flux and the \bar{p}/p flux ratio poses the challenge of achieving a similar precision in phenomenological models that describe the CR \bar{p} flux as produced by the interaction of the CR primary components with the Interstellar Medium.

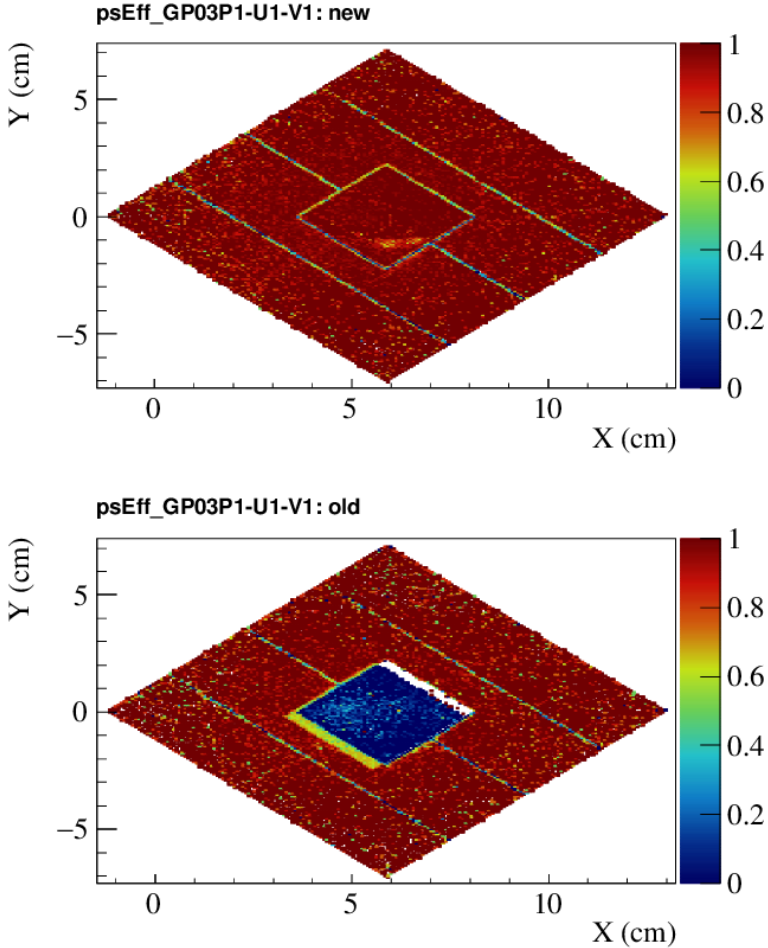


Fig. 13: Pseudoefficiency of the Pixel GEM 2 station, U and V plane obtained for two different iterations of the alignment procedure of one run at 190 GeV/c. In the top figure the most updated result is shown.

Table 3: Summary of decay channels used to compute PID efficiencies.

Hadrons	Decays	
	Channel	BR (%)
K_S	$\pi^+ \pi^-$	(69.20 ± 0.05)
ϕ	$K^+ K^-$	(48.9 ± 0.5)
$\Lambda(\bar{\Lambda})$	$p\pi^- (\bar{p}\pi^+)$	(63.9 ± 0.5)

Currently the large uncertainty on the antiproton production cross section is one of the main sources of models uncertainty. In order to cover all of the AMS-02 \bar{p} energy range, precise $p + p \rightarrow \bar{p} + X$ and $p + {}^4\text{He} \rightarrow \bar{p} + X$ cross-section data are needed in a wide proton-beam energy range from 10 GeV to a few TeV. The very first data set on $p + {}^4\text{He} \rightarrow \bar{p} + X$ has been collected in May 2016 by the LHCb collaboration at 6.5 TeV beam energy ($\sqrt{S_{NN}} = 110.5$ GeV), operating the SMOG target with helium gas. Similar measurements at 4 TeV are foreseen by LHCb. AMBER collected this year unique data set on $p + {}^4\text{He} \rightarrow \bar{p} + X$ in the unexplored beam momentum range of 60–250 GeV, which is with no doubt the signature contribution of our approved proposed program.

More data sets and results are available on $p + p \rightarrow \bar{p} + X$, the most recent ones from the NA61 collaboration at 20, 31, 40, 80 and 158 GeV [4]. Nevertheless, as already mentioned in the approved AMBER proposal [3], performing a new measurement on $p + p \rightarrow \bar{p} + X$ having a large overlap with the already available ones would allow for a direct comparison of the results and for an important study of possible systematic effects.

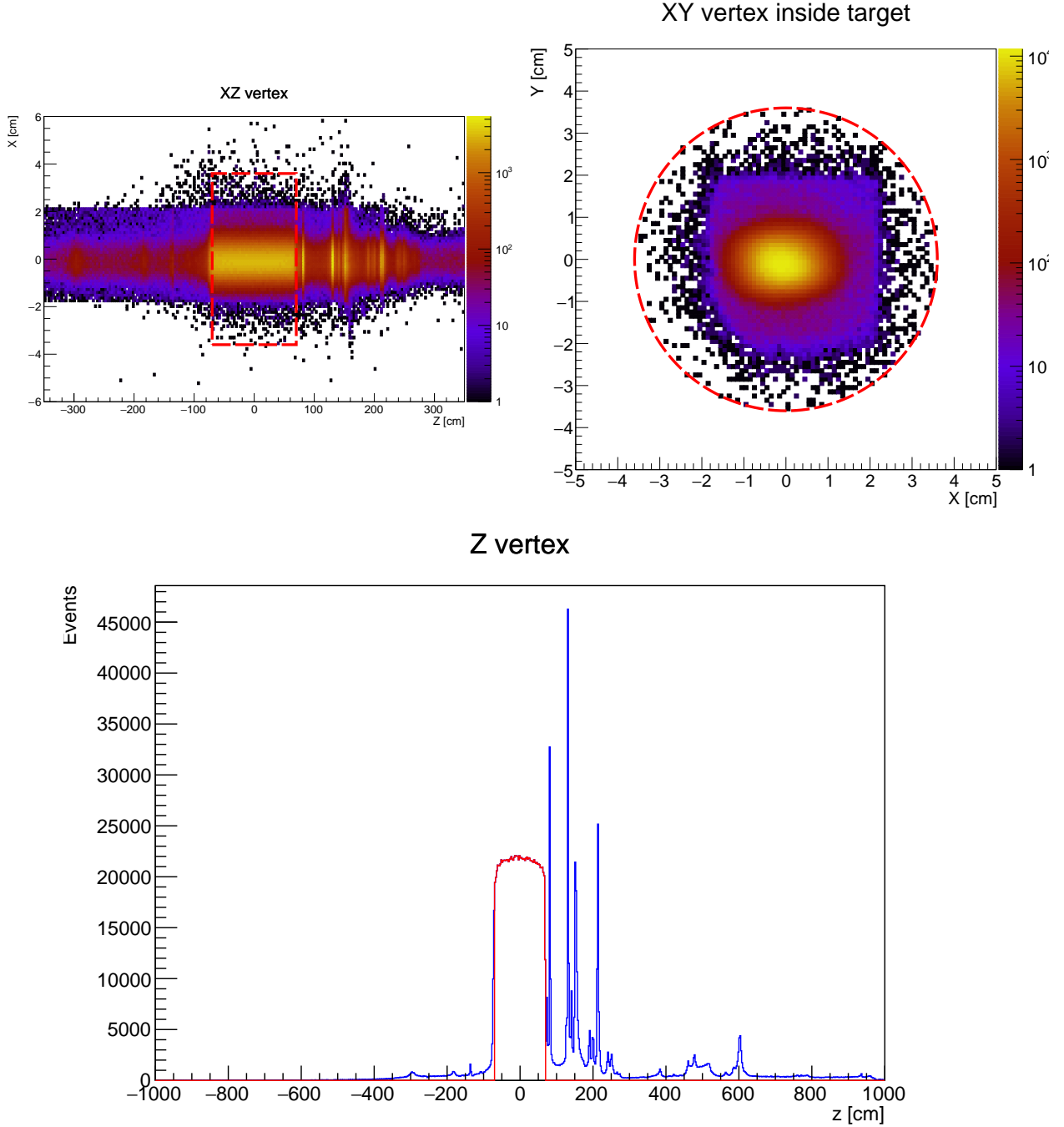


Fig. 14: Top: $x - z$ and $x - y$ primary vertex spatial distribution from a sub-sample of one run in period W01 (at $190 \text{ GeV}/c$). The dashed line shows the dimension of the target along $x - y - z$. Bottom: in red the effects of cutting on target dimension on the z distribution of primary vertices. Preliminary, work in progress.

The AMBER data will also extend the NA61 coverage on large transverse momenta. In Fig. 17 the transverse momentum \bar{p} spectra in rapidity slices published by NA61 for inelastic $p + p$ interactions at 158 GeV are compared with a projection of the results expected at AMBER at 160 GeV .

Furthermore, recently the theoretical astro-particle physics community highlighted the need for new data on the inelastic production cross section $p + p \rightarrow \gamma + X$ in the π^0 production channel [7]. The flux of γ rays in the universe has been measured by the Fermi Large Area Telescope with unprecedented precision in the last fifteen years over the full sky coverage in an energy range from 100 MeV up to about 1 TeV . In order to be able to accurately interpret these data a similar precision has to be achieved on the prediction of the production cross-section of γ rays from the interaction of cosmic-rays (mostly proton and helium) with the ISM. In par-

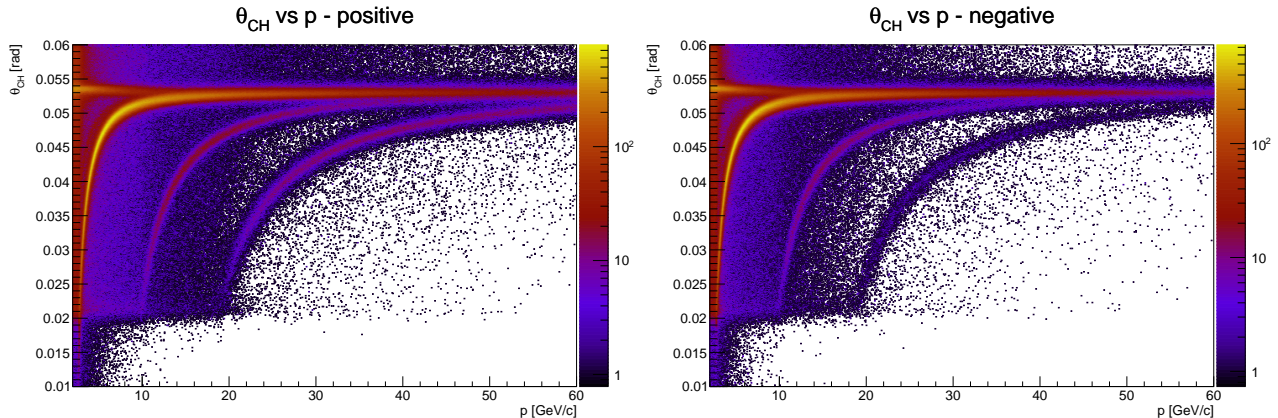


Fig. 15: Cerenkov angle in RICH-1 produced by positive particle (left) and negative particles (right) as a function of momentum. Preliminary, work in progress.

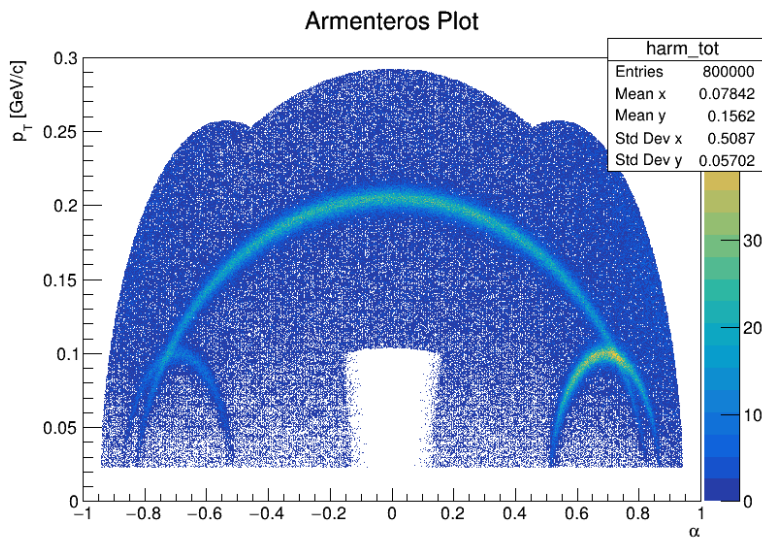


Fig. 16: Armenteros-Podolanski plot: on the y -axis the p_T of one daughter particles from the V0 decay vs the longitudinal momentum asymmetry. The main arc band represents the population of $K0s$ and the two smaller arcs are the Λ and $\bar{\Lambda}$. Preliminary, work in progress.

ticular, the main production mechanism for γ rays is the π^0 decay. But data on $p + p \rightarrow \pi^0 + X$ are scarce, with a limited kinematic phase space coverage or affected by large systematic uncertainty. The π^0 production cross-section is currently modelled from the π^\pm production cross-section, resulting in large systematic uncertainties. Therefore further experimental measurements of the neutral pion production in hadronic collisions are encouraged. AMBER may perform a measurement of the $p + {}^4\text{He} \rightarrow \pi^0 + X$ with the data already collected this year. For this reason the Electromagnetic Calorimeters (ECALs 1 and 2) were commissioned, calibrated and kept operational for the 2023 run. Nevertheless a measurement on $p + p \rightarrow \pi^0 + X$ would certainly be of great interest, even if not the flagship measurement of our experiment.

The running strategy for 2024 of a measurement on $p + p \rightarrow \bar{p} + X$, which is already part of the approved AMBER proposal, has been discussed inside the AMBER collaboration. An extraordinary Technical Board meeting has evaluated positively the feasibility of such a measurement during the first half of 2024 and the proposal has been unanimously approved by the Collaboration Board in July. Two months of data taking would be foreseen to collect data with positive hadron beam at at least four different momenta (80, 160, 190, 250 GeV) impinging on a Liquid Hydrogen Target 140 cm long. The equipment for the LH₂ target is fully available, except for the target cell itself. Fortunately, CERN TE-CRG group has deep knowledge and experience in designing and building a new target cell and in the construction of a liquid H₂ target. Supportive comments were expressed by the TE-CRG group when we had first discussion with them on the liquid H₂ target. It

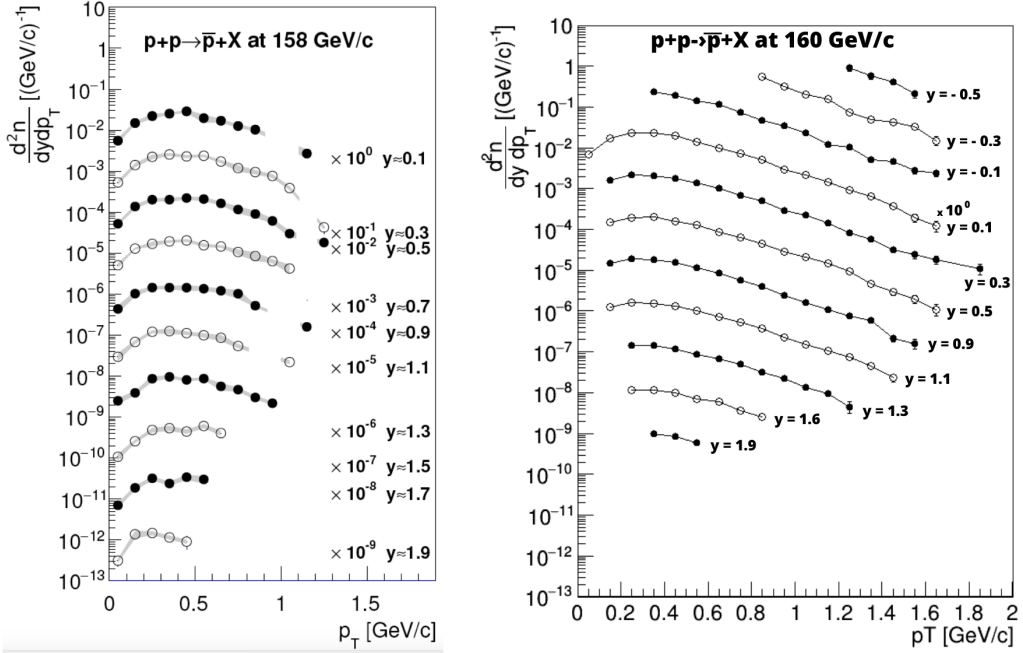


Fig. 17: Transverse momentum \bar{p} spectra in rapidity slices produced in $p + p$ inelastic interactions at 158 GeV by NA61 (left figure) [4]. For comparison the expected results obtainable by AMBER in $p + p \rightarrow \bar{p} + X$ at 160 GeV are shown (right figure).

has been estimated that about six months will be needed for the realisation, therefore design specification are needed by mid of September. For the rest, the same spectrometer setup as in 2023 will be used.

3 Proton Charge-Radius Measurement

We present an update on the progress with respect to the previous report [1] summarised for the SPSC in 2022. As a follow-up on the presented preliminary results on the 2021 Time Projection Chamber (TPC) tests at the M2 beam line in the so-called CEDAR region with a close-to-final layout of the setup, we present the promising result (c.f. Sec. 3.1) of the combined data taking based on a common time stamp using the IKAR TPC as down-scaled version of the anticipated final TPC (c.f. Sec. 5.1) and the existing silicon-microstrip tracker system. Furthermore, developments of the Universal Tracking Station (UTS) detector systems (Scintillating Fibre Hodoscope, SFH and Silicon Pixel Detector, SPD) (c.f. Sec. 5.2) have been performed. Those developments have been tested during a dedicated beam test in 2022 (c.f. Sec. 5.2.1) and we present results of the SFH and SPD individually. Those served as input for further improvements which have been further evaluated during a parasitic beam test of the SFH during the antiproton production cross-section measurement during the first half of 2023 and preliminary results for the prototype developments show important improvements in the uniformity of the light-yield per channel and fiber alignment. For a evaluation of the full-scale setup including the new streaming DAQ system and novel detector front-ends, a dedicated beam test in September with four partially equipped UTS stations and the IKAR TPC is in preparation (c.f. Sec. 3.2). The obtained results of these tests are combined with the ongoing developments and can lead towards a possible physics pilot run in 2024 with a main data taking that could follow in 2025 according to the time schedules (c.f. Sec. 3.3).

3.1 Results from the 2021 Pilot Run

In the previous SPSC report [1], first preliminary results of the IKAR TPC test in 2021 at the M2 test beam location (CEDAR position at M2) were presented. During those 20 days of dedicated beam time, the down-scaled version of the final TPC (c.f. Sec. 5.1) with an operational pressure of up to 8 bar was tested together with a close-to-final layout of the surrounding tracker system and the muon beam optics. The TPC and the tracking system were operated in two distinct DAQ systems. A common so-called TRLO time stamp was used to allow a later combination of the data on an event-by-event basis. The main goals of the test was to evaluate

the TPC performance in a focused muon beam with the proposed rate of 2 MHz and to study rate dependence of the energy resolution due to the beam-induced noise with the proposed new pad-plane structure.

Already the presented preliminary results showed that the beam-induced noise in the TPC remained below the required 40 keV even for beam rates up to 5.6 MHz at a hydrogen pressure of 7.5 bar. This reflects also positively on the single pads energy resolution of the tested new pad-plane structure and allows a clean signal extraction. [1]

During the combined operation with the TPC, about $1.6 \cdot 10^9$ tracking events have been recorded as shown in Fig. 18(a). About $3 \cdot 10^5$ events are selected from those to be combined with the recorded TPC events on a later stage. The time stamp creation started at run number 293218 and spill number 67. From there on we obtained a full coverage of the combined data in terms of the common time stamp for all recorded spills and runs as shown in Fig. 18(b). For each spill in each run the number of synchronisation ticks for the common time stamp is shown. Around 5 to 7 synchronisation ticks are expected based on the given implementation of the time stamp protocol. The maximum number of recorded spills per run is indicated (red) to visualise the coverage.

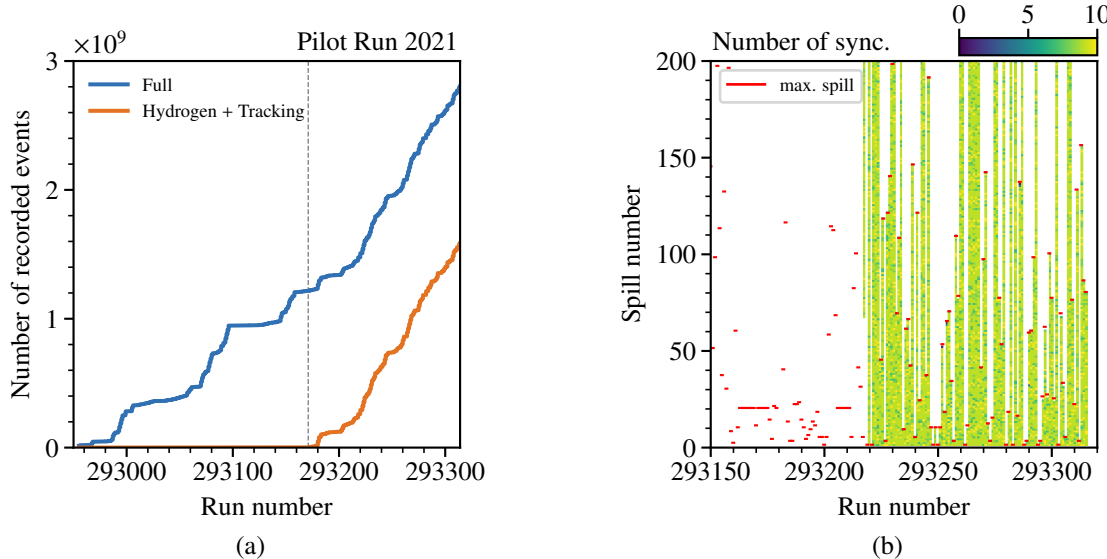


Fig. 18: The integrated number of events during the pilot run is shown in (a). In (b) the number of synchronisation ticks used for the TRLO time stamp is presented. [8]

In Fig. 19(a) the calibrated and corrected energy spectra of the measured IKAR TPC data is shown. The calibrated off-spill data (green) is used to subtract the contribution of the α calibration-source in the on-spill data (orange) to obtain the corrected (blue) energy distribution. The off-spill data is scaled based on the duty-cycle between on- and off-spill events. The influence of the α -source is visible around an energy of 5.486 MeV (^{241}Am). Two sources are placed on grid and cathode, respectively. The attenuated contribution of the cathode source due to gas attachments along the drift towards the readout plane is visible. Further calibrations are required to obtain a clean energy distribution. Especially, attachment processes along the drift need to be corrected based on the vertex z -position. [8].

Using the TRLO time stamp to select measured events in the TPC as well as the tracking system within the TPC drift time window of about 150 μs results in the correlation time peak shown in Fig. 19(b). A total of 1974 correlated events have been selected and show the expected flat time window distribution. Those events show similar, but much more pronounced correlations compared to the 2018 feasibility test in energy and vertex position. In Fig. 19(c) the total measured energy in the TPC of those correlated events is shown with its dependency on the Q^2 , which is proportional to $\sin^2(\theta/2)$. The correlation between the drift time and the

z -vertex position in the TPC is shown in Fig. 19(d). The two 40 cm long drift volumes are visible and show the expected time-position dependence due to the drift towards the anodes.

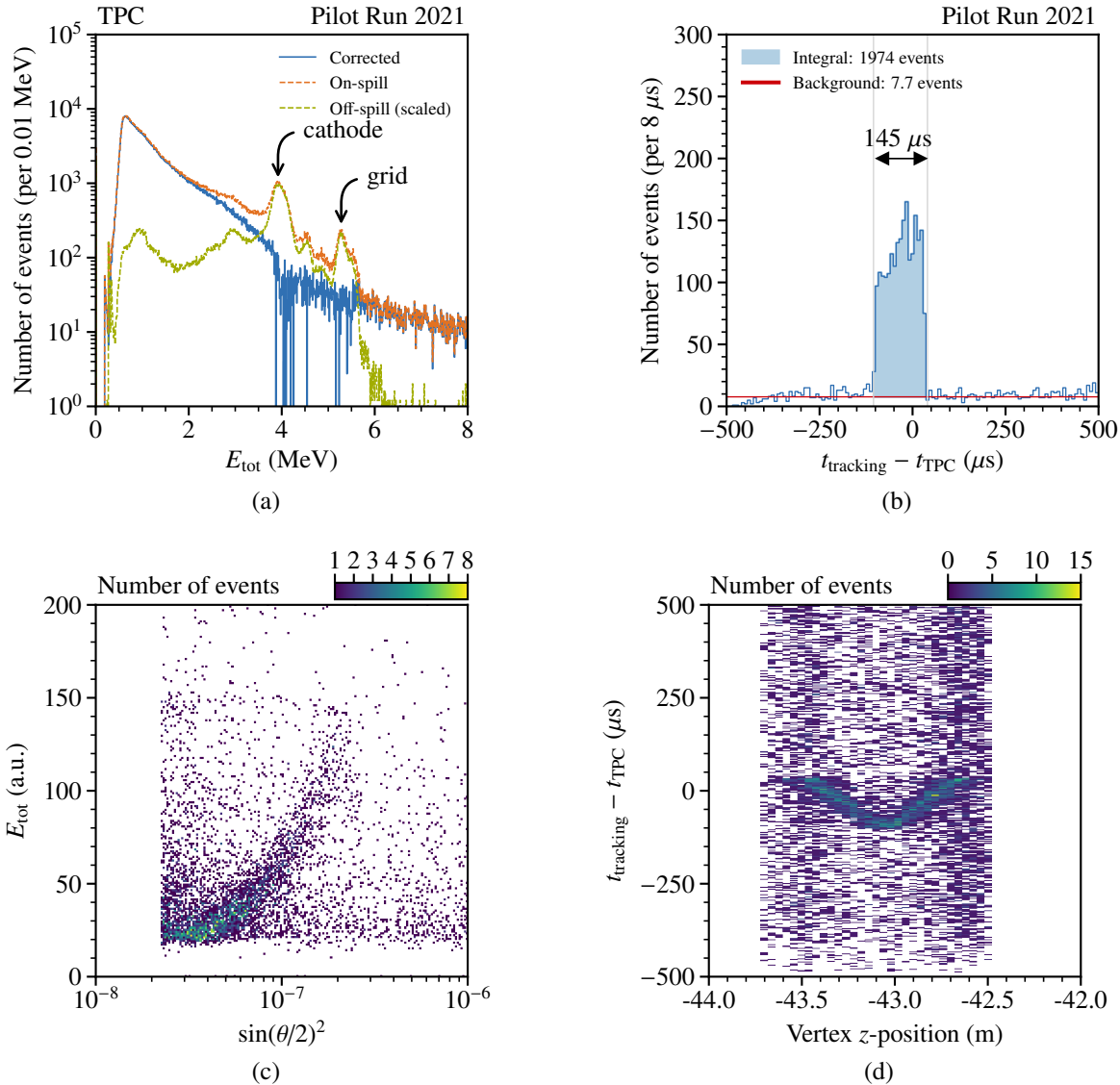


Fig. 19: In (a) the extracted TPC energy spectrum is shown. The TRLO time stamp difference between the tracking and TPC system is shown in (b) with the resulting correlations in energy and vertex position shown in (c) and (d). [8]

For the absolute calibration of the measured beam momentum using the data also recorded of the Beam Momentum Stations (BMS) upstream in the M2 beam line, the elastic muon-electron scattering can be used as already presented in the previous report [1]. Selecting events originating from the beam window structures of the TPC show the angular correlation of the muon and electron scattering angle as shown in Fig. 20(a). Compared to the previous analysis based on the 2018 feasibility test data, the incoming beam momentum was known and fixed to about 100 GeV resulting in a clean correlation. Due to the missing particle identification, the shown data is symmetrically and no distinction between muon and electron could be done. Nevertheless, using the kinematic relation between both angles, the expected energy of (99 ± 4) GeV could be extracted using the small obtained data set as shown in Fig. 20(b). The extraction of the beam momentum can then later be used to calibrate the measurement of the BMS station. Based on simulation and systematic studies we investigated the

requirement of the beam energy resolution $\sigma_E < 0.1\% \cdot E_\mu = 0.1$ GeV for a sufficient calibration to extract the proton charge-radius r_p with an absolute precision better than 1 %. As shown in Fig. 20(c), we do not observe systematic shifts larger than $\sigma = 0.1$ of the extracted mean value above 10 batch sizes of 10^3 events each.

A combined reconstruction of the setup including the TPC setup and the spectrometer was tested and will be further studied in the future. Using this reconstruction, tracks could be matched between the TPC setup region and the spectrometer positioned around 40 m downstream. The challenge is to bridge these tracks over magnets along the M2 beam line towards the spectrometer. The momentum reconstruction of the scattered particle by using one spectrometer magnet (SM2) only was successfully tested, yielding the expected average beam momentum as shown in Fig. 20(d). For the momentum reconstruction of the incoming particle by the BMS, a new algorithm based on a Neural Network was used for the first time, showing promising results. The model was trained on low-scattering tracks with a momentum reconstructed in the spectrometer.

Further steps are to refine the method to include also the measured BMS information to verify and apply the presented method. Together with the usage of particle identification based on the combination with the spectrometer allows a distinction between muon and electron tracks. Furthermore, the extraction of the measured momentum of the scattered muons could allow an evaluation of the combined measurement of the elastic scattering using the recoil proton and the scattered muon.

3.2 Ongoing Activities and Plans for 2023

With the ongoing activities in detector developments, various tests have been performed. Prior to the 2023 PRM beam test, a parasitic test of the SFH prototype was performed at the test stand location upstream of the M2 beam dump. The preliminary results of this test are presented in the following. Furthermore, a dedicated beam test of the close-to-final PRM setup is scheduled during September 2023 and preparations are ongoing. The current status and plans are further described in Sec. 3.2.1.

3.2.1 Status and Plans for the 2023 Beam Time

Preparations of the spectrometer and especially the target region for the 2023 PRM beam test are ongoing. The target setup of the preceding antiproton production cross-section measurement has been already removed and the gained space is to be used to construct the target setup with the IKAR TPC and UTS vessels for the PRM part. The time line for the PRM beam test preparation is shown in Fig. 21. The PRM commissioning phase consists out of the installation and preparation of the new target platform, which provides the support for the TPC and UTS. An early TPC installation is required to proceed with the installation of the safety critical hydrogen lines. In the beginning, the TPC will be operated with helium to perform first tests and measurements. After the safety clearance for hydrogen, the TPC can be operated under nominal conditions.

The IKAR Time Projection Chamber (TPC) underwent preparations for its operational phase commencing in early August. These preparations encompassed the establishment of an optimal vacuum condition during the initial stage, followed by subsequent refinement through a series of clean nitrogen flushing processes. During this phase, the IKAR TPC was introduced to a minute quantity of gas (at a pressure of several millibars), which was subsequently evacuated. Iterative execution of this procedure facilitated the elimination of residual air and moisture, which may have been introduced during the TPC's previous maintenance period.

Following its preparation, the IKAR TPC underwent testing within the designated preparation area. It was charged with a gas mixture composed of 90 percent helium and 10 percent nitrogen. The experimental assessment of the system involved the utilisation of alpha particle sources positioned at the cathode and grid locations. The purpose of these tests was to evaluate the setup's performance by quantifying the energy of the

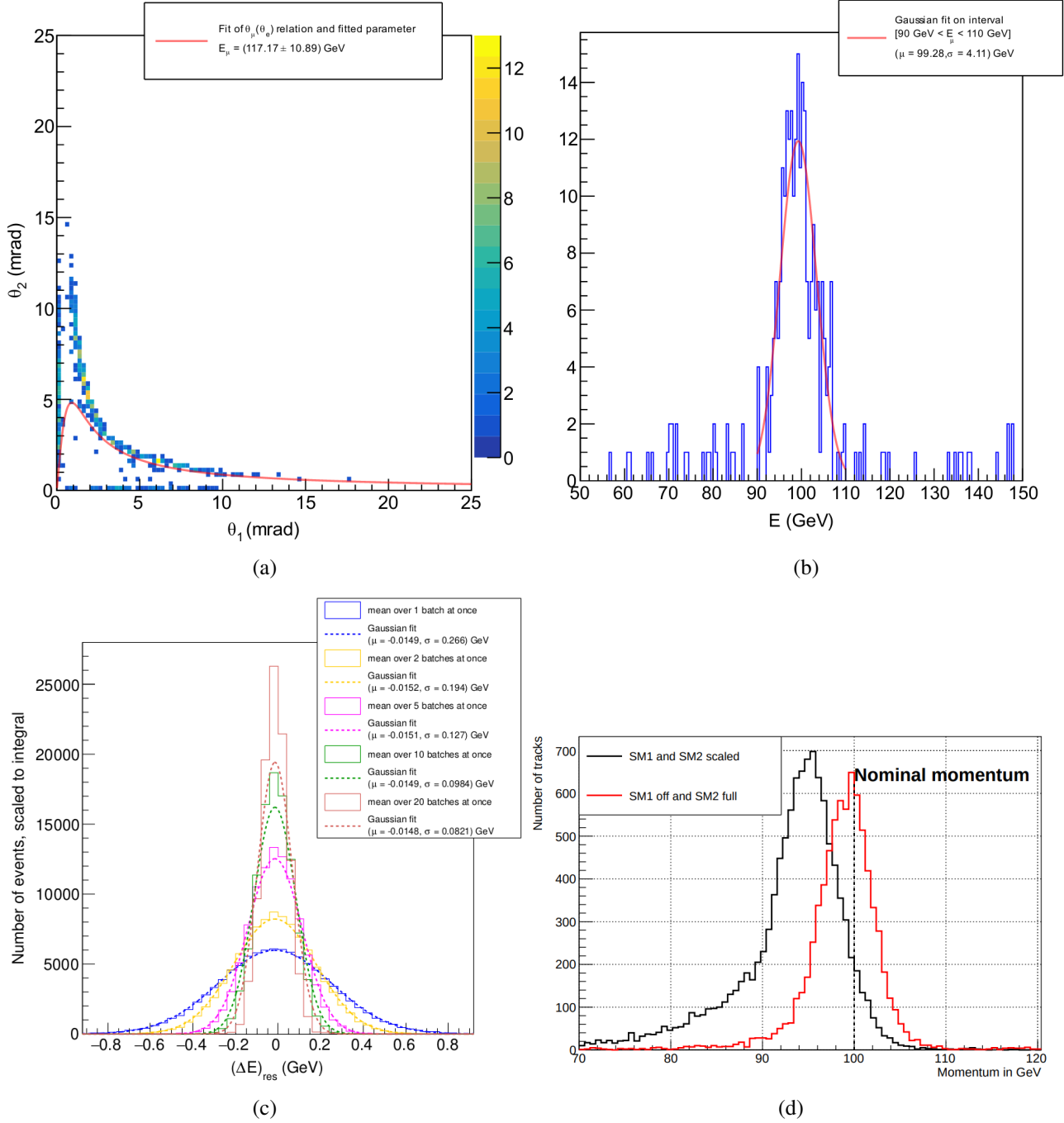


Fig. 20: In (a) the angular correlation between muon and electron is shown with the extracted incoming beam momentum presented in (b) and the systematic studies for the momentum precision are shown in (c) [9]. In Fig. 20(d) the reconstructed momentum using different spectrometer options is shown [10].

emitted alpha particles. The ionisation process initiated by the alpha particles originating from the cathode source led to the generation of ionisation electrons. These electrons traversed the gas-filled chamber, potentially undergoing capture by gas admixtures. In contrast, the majority of electrons generated by alpha particles originating from the grid-source reached the anode without substantial interaction. Comparative analysis of the maximum recorded energies of alpha particles emitted from the cathode and grid sources indicated that electron attachment during the drift within the gas cell had already reached a level of approximately 5 percent. Further enhancements in this regard are anticipated in the immediate future.

Concurrently with the preparation of the ionisation chamber, a specialised campaign aimed at calibrating the pre-amplifier has been initiated. This campaign entails both the relative measurement of amplification coeffi-

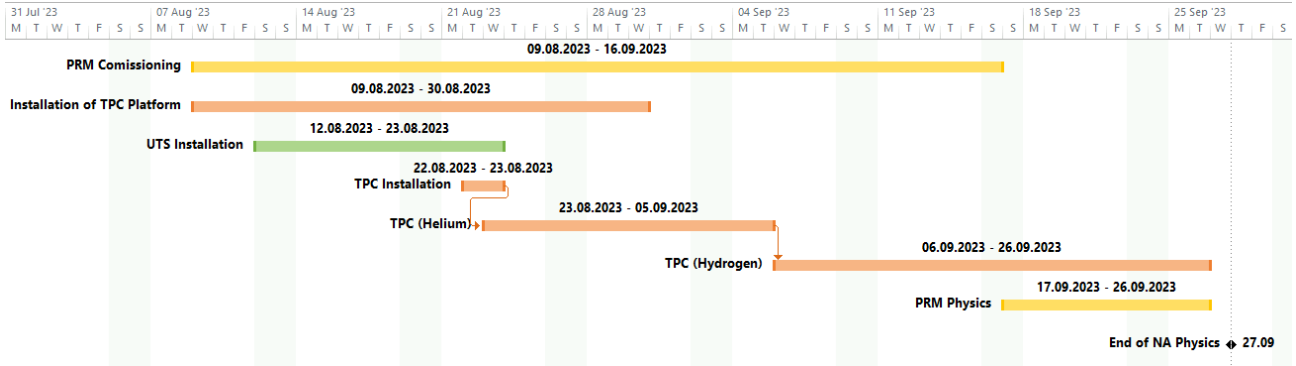


Fig. 21: Anticipated timeline for the PRM beam test preparation in 2023. TPC and UTS installation and the operation times are indicated.

cients across distinct readout channels and absolute calibration procedures. In the latter approach, a generator pulse traverses through a calibrated capacity. This allows the discernment of the amplifier's response to a known electric charge, enabling the establishment of a correlation between this response and the ionisation energy deposited within the chamber. The comprehensive calibration process encompasses several steps: an assessment of non-linearity in amplification coefficients concerning initial energy pulses, an examination of temperature-dependent effects, and the evaluation of noise introduced by the pre-amplifier. Furthermore, noise measurements will be conducted on the installed amplifiers across various operational modes. This will encompass scenarios involving both high voltage (HV) deactivation and activation, as well as the interchange of amplifiers within the TPC.

In Fig. 22 a detailed sketch of the PRM beam test setup for 2023 is shown. The IKAR TPC will serve as active target and is centered between two partially equipped UTS stations along each lever arm on the up- and downstream side. Each of the UTS is equipped with a SPD prototype. The currently existing SFH prototype will be mounted in one of the UTS as well. As reference detector, two existing AMBER SciFi (SF) are placed along each lever arm. From the spectrometer side, all detector equipment compatible with the new streaming DAQ will be used. This includes novel GEM detectors, SciFis, MWPCs. This allows a full-scale test of the new DAQ and reconstruction software.

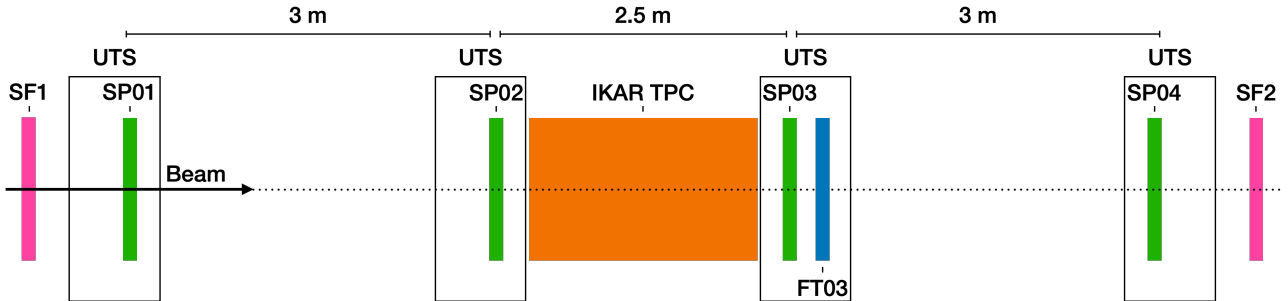


Fig. 22: Sketch of the PRM beam test setup for 2023. The IKAR TPC (orange) is centered between two UTS stations along each lever arm up- and downstream each equipped with SPD prototypes and one with the SFH prototype. Existing SciFi (SF) detectors (pink) are placed along each lever arm.

The goals for the beam test focus mainly on the new components and their combination and can be summarised as follows:

1. Installation and commissioning of TPC infrastructure and safety installations
2. Installation and commissioning of new UTS vessels including SFH and SPD detector with their new readout electronics
3. Commissioning of new streaming DAQ together with new detector front-end electronics

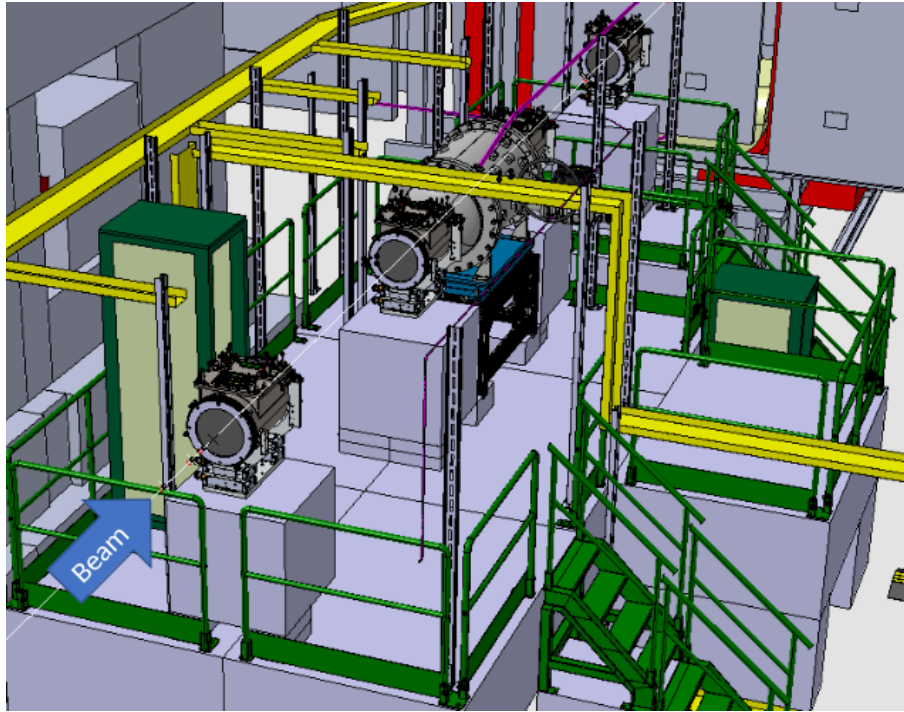


Fig. 23: Sketch of the target area for the PRM beam test in 2023 with the beam entering from the lower right-hand side. The UTS are placed on separate concrete blocks up- and downstream of the central IKAR TPC. Cable tray (yellow) positions are indicated as well as hydrogen lines (purple).

4. Verification of monitoring tools and calibration processes for DAQ and detector components
5. Data reconstruction in the new data format of the streaming DAQ
6. Study of detector efficiencies and resolutions at different beam rates up to 10 MHz

3.3 Plans for 2024/2025

Based on the experience obtained during the beam test in 2023 as described in Sec. 3.2.1, the close-to-final setup for the PRM measurement could be constructed in 2024 using the majority of the final parts and detector components with the respective electronics. Main feature would be the novel TPC as upgrade of the currently used IKAR TPC. A test run of the measurement should take place, presumably in the of 2024 SPS proton Run, as final preparation towards a physics run in 2025. Main objectives would be extensive detector and DAQ tests as well as resolution and acceptance studies of the foreseen setup as shown in Fig. 24. The obtained results should provide first physics-related insights in terms of a possible extraction of the proton radius, but with a limited statistics. Required improvements could be performed towards 2025.

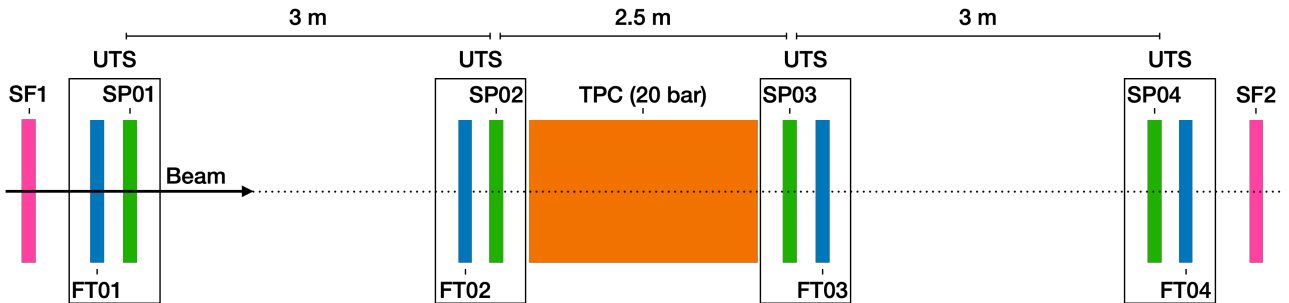


Fig. 24: Sketch of the foreseen 2024/2025 setup with the final TPC and all four UTS equipped.

4 Meson structure measurement by using Drell-Yan process

4.1 First results of the Cherenkov detectors (CEDAR's) test with high intensity hadron beam.

As presented in the previous report [1], the CEDAR detectors are a crucial element of the Drell-Yan (DY) setup. These detectors located in the M2 beam line upstream from the target region of the spectrometer identify the beam particle. The basic principles for the identification were explained in section 2. There are several challenges when operating the CEDAR detectors: the beam divergence at CEDAR location, the uncertainty on the reconstructed beam particle parameters, the high beam intensity required by the Drell-Yan measurement, the noise level seen by the CEDAR PMT induced mostly by the beam halo which produces Cerenkov radiation when hitting the PMTs windows. The beam trajectory, measured by the beam telescope detectors, is reconstructed and extrapolated to the upstream region, since there are no tracking detectors at the CEDARs location. This extrapolation is done using a beam transport matrix, obtained from dedicated simulations using the MADX package. Six transport matrices were prepared by the Beam group (BE/EA) reflecting the different optics used for the beam energies: 60, 80, 100, 160, 190 and 250 GeV. In 2023 a CEDARs test was performed, to address the challenging conditions of the CEDARs in Drell-Yan measurement conditions. The test took place immediately after the antiproton cross section measurement Run and lasted from 30 June to 4 July. In order to improve the space resolution of the beam telescope the much more precise silicon tracking detectors (3 stations of 4 planes each) were added to the usual scintillating fiber detectors (7 tracking planes), in a setup similar to that of the antiproton Production Cross-Section Measurement (APX). The planning of the performed test was started with simulations performed by the CERN Radiation Protection group (HSE-RP). The goal was to assess the possibility of using high beam intensity, as in the COMPASS DY 2018 Run, but without the presence of the Hadron Absorber in the setup (that could not be assembled due to time constraints). The Helium target container used during the APX measurement, although empty was still in place. The results for the simulations performed in FLUKA, considering $3.5 \cdot 10^8$ particles per spill (the nominal beam intensity in 2018) with two spills in a 28.8 s super-cycle are presented in Fig. 25. It can be observed that with this intensity in the current setup, the region nearby the beam dump downstream of the spectrometer, indicated by the red line, exceeds the radiation dose allowed limits, thus the area had to be classified as *prohibited* during the period of the test.

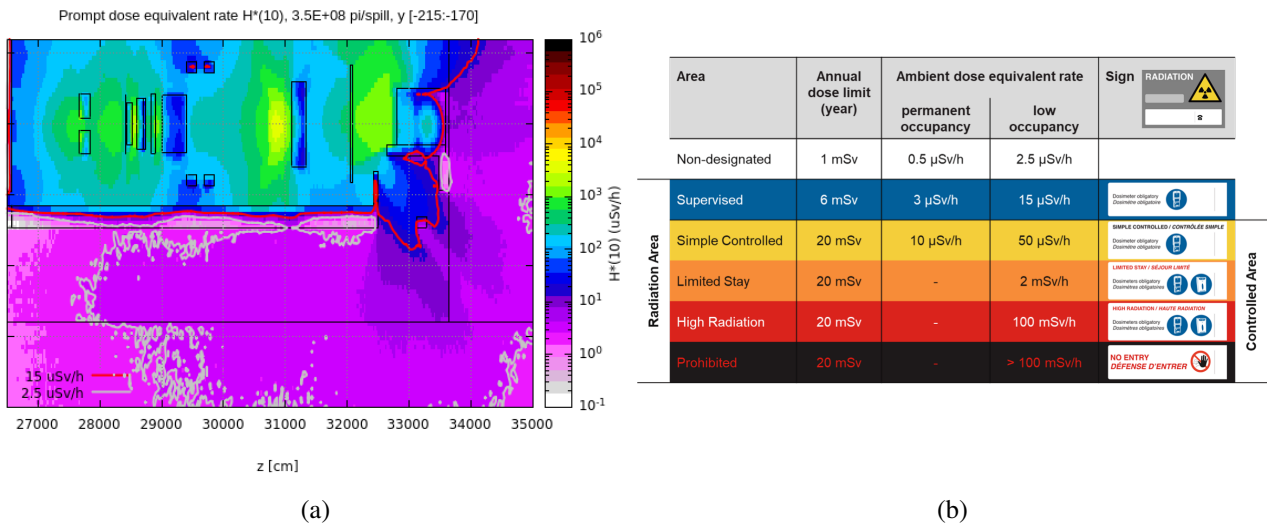


Fig. 25: In (a): Prompt dose equivalent in EHN2 and beam dump area. In (b): Table of radio-protection designated areas and their respective limits.

These simulation results were confirmed by *in situ* measurements performed immediately before the test, on the 30th June. Based on the measurement, the RP group established the following conditions:

- Temporary exclusion zone at the outside neighbourhood of EHN2

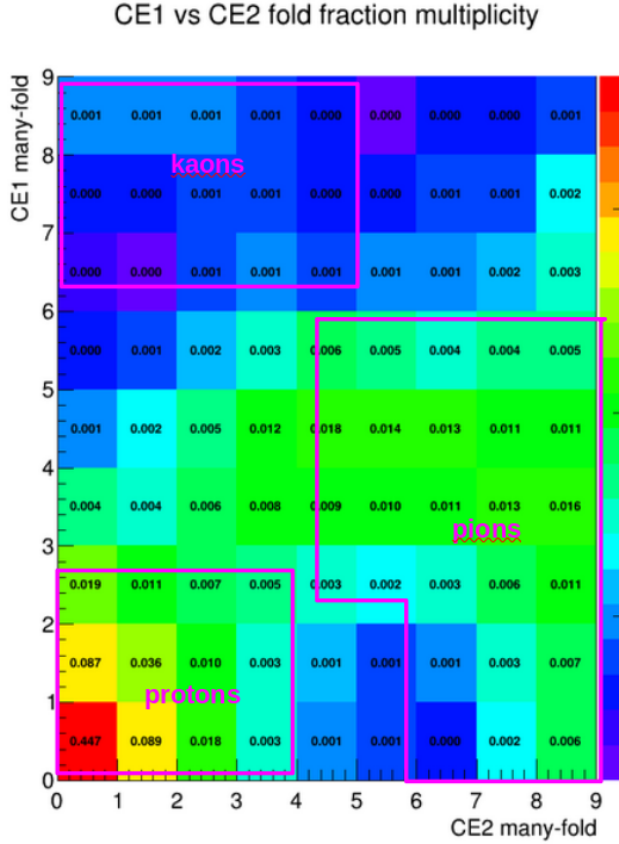


Fig. 26: CEDAR1 versus CEDAR2 multiplicities, for positive hadron beam of 190 GeV, with CEDAR1 tagging kaons and CEDAR2 tagging pions.

- Maximum beam intensity allowed only during night
- High-intensity maximum value: $3.5 \cdot 10^8$ particles per spill
- Maximum beam intensity allowed during the day: $7 \cdot 10^7$ particles per spill

In order to run the CEDAR detectors at high intensity, the firmware of TDCs was adapted and a digitizer was set upstream of CEDAR1 in order to study and check the individual PMTs signals. Data was acquired for several conditions:

- Positive and negative hadron beams at intensity of $7 \cdot 10^7$ and $3.5 \cdot 10^8$ particles per spill at 190 GeV
- Negative hadron beam at 160 GeV
- Both CEDAR detectors tagging the same particle, pions or kaons
- CEDAR detectors tagging different particles, i.e., one tagging pions while the other tagged kaons
- Several CEDAR detector pressure scans and alignment with low intensity hadron beam.

In Fig. 26 the online response on CEDAR1 vs CEDAR2 multiplicities (i.e. PMTs giving signal) is shown for the positive hadron beam at 190 GeV momentum. In this case, CEDAR1 was set on the kaon peak and CEDAR2 on the pion peak. The regions where pions and kaons are identified are clearly visible, even without any further data treatment. The large statistics accumulating in the region where none of CEDARs gave signal are protons.

Unfortunately, the CEDAR detector alignment was limited to $100\mu\text{m}$ due to a known issue in the moving motors that could not be fixed on time. Moreover, the CEDAR detectors diaphragm motor was also impossible

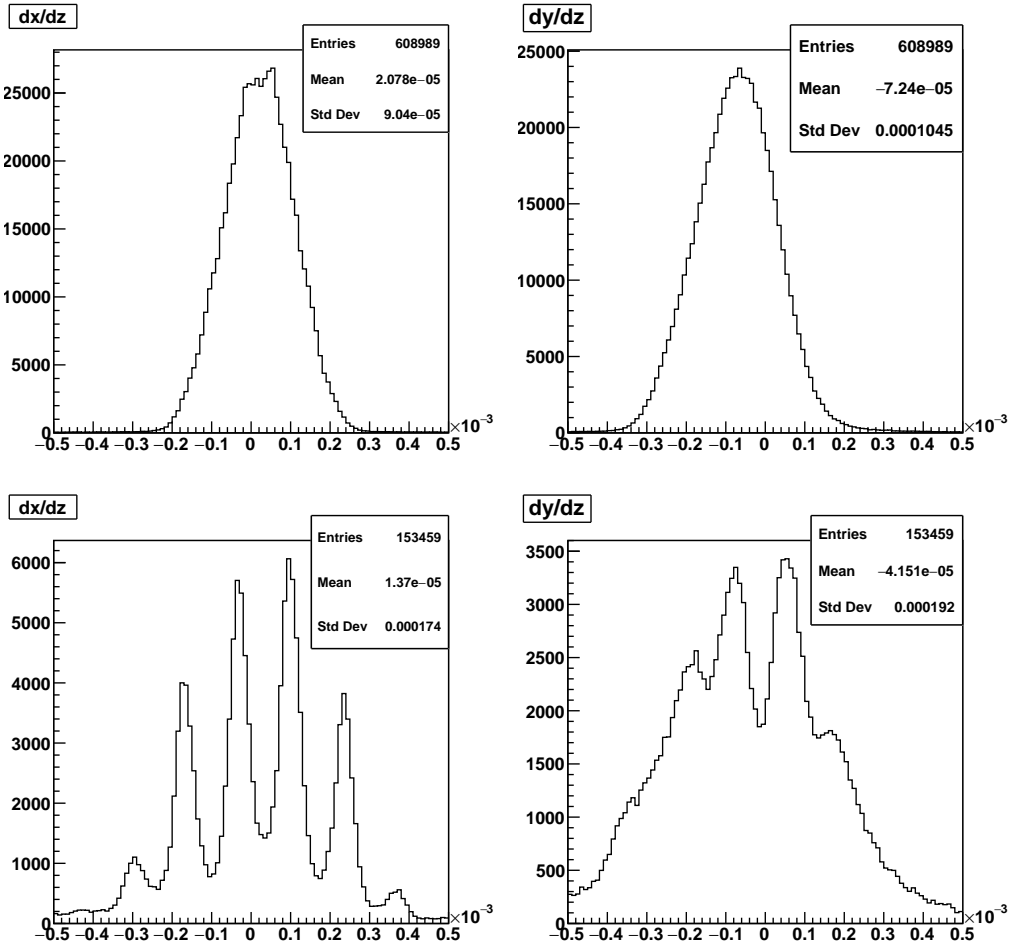


Fig. 27: Comparison of the beam angles dx/dy and dy/dz (in rad) at the beam telescope ($Z = -440$ cm) between 2023 DY test (top) and 2018 COMPASS DY (bottom). Preliminary, work in progress.

to control, preventing the planned studies varying diaphragm aperture. For the moment the analysis of the data is just starting. Part of one run with 190 GeV positive hadron beam of relatively low intensity (44×10^6 particles/spill) was analysed. The beam tuning in 2023 lead to a clear reduction in the beam divergence (at least for the 190 GeV positive hadron beam case). The addition of the silicon detectors in the beam telescope, on the other hand, had the expected positive impact to the beam reconstruction. Fig. 27 shows the comparison of the beam angles dx/dz and dy/dz at a location $Z = -440$ cm (half-way in the beam telescope), between 2018 DY data-taking and 2023 DY test. The spikes in the 2018 distributions were due to the lack of angular resolution.

Fig. 28 presents the response of the 8 PMTs of CEDAR2, which was tuned on the kaon peak. The most prominent yellow bands show the pions, while the kaon band appears less visible given its comparatively low fraction in the beam, in green. The color scale was limited to 0.25 which is the expected pion content on the positive beam at 190GeV.

The same is depicted in Fig. 29, but this time in 1D, as a function of the particle's angles at CEDAR2 dx/dz (left) and dy/dz (right), in this case obtained from the response of only 2 PMTs. The peak shown at larger positive angle, reaching a fraction of 24 % are pions. A much smaller fraction of kaons is shown at the angles close to 0, while the proton peak, most abundant, is visible on the left, at most negative angles.

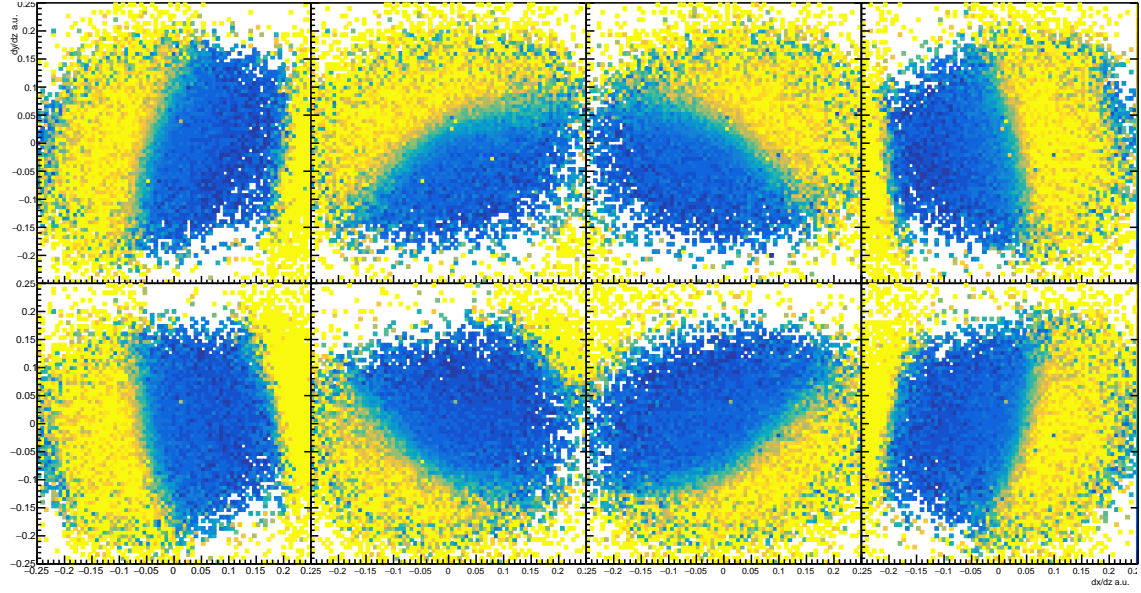


Fig. 28: Response of the CEDAR2 PMTs normalized to the beam flux in bins of beam slope when having 190 GeV positive hadron beam at intensity of 44×10^6 particles/spill, and the CEDAR tuned on the kaon peak. Color scale from 0 (dark blue) to 0.25 (yellow). Preliminary, work in progress.

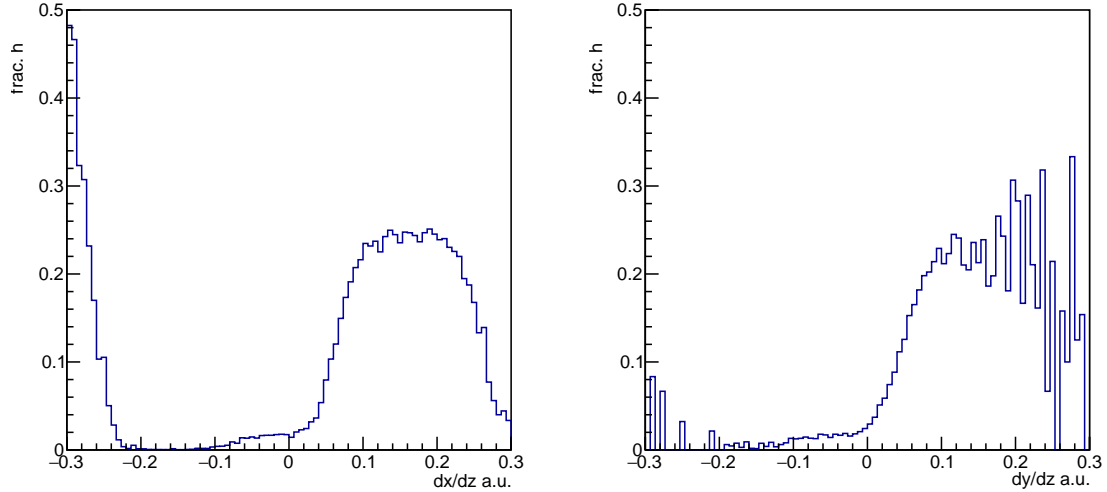


Fig. 29: CEDAR2 particle identification, when having 190 GeV positive hadron beam at intensity of 44×10^6 particles/spill, and the CEDAR tuned on the kaon peak (only 2 of the PMTs used here). Preliminary, work in progress.

5 Hardware

5.1 TPC and Gas System

5.1.1 Preparation of the IKAR TPC for 2023

For the preparation of the beam time in September 2023, the IKAR TPC will be commissioned starting from beginning of August 2023. This involves the vacuum system consisting out of the vacuum pumps and sensors as well as the big pressure valve. A sketch of the preparations is given in the timelines shown in Fig. 21. A main part of the installation work this year are the safety aspects of the hydrogen operation in the target area of the spectrometer. This includes mounting of the respective hydrogen lines and safety elements with the required checks of all connections. Furthermore, the gas filling system for the TPC using either Helium or Hydrogen

has to be assembled at the new location as shown in Fig. 30.

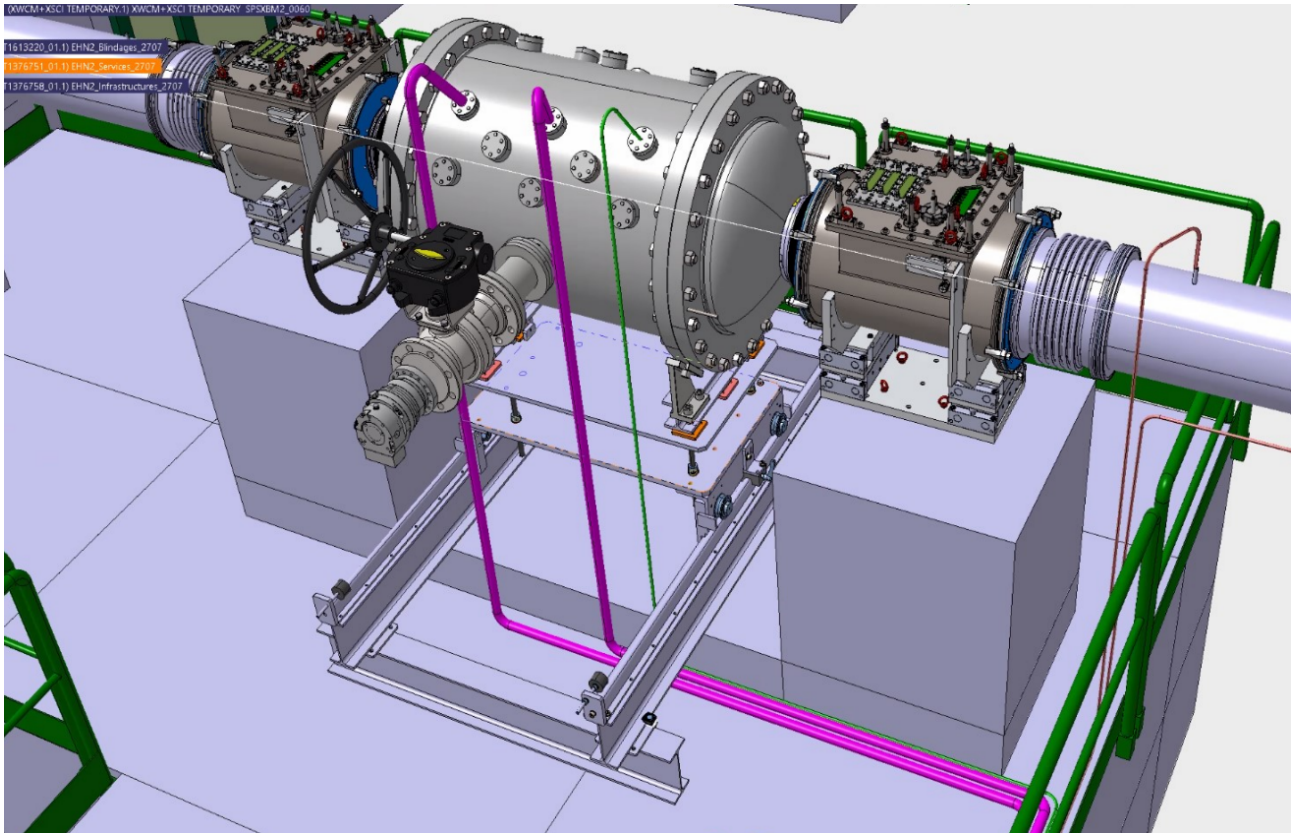


Fig. 30: Sketch of the foreseen IKAR TPC preparations in the target area sandwiched between two UTS. Hydrogen lines are indicated in purple.

For the hydrogen gas system, the installations of the 2021 setup will be reused as shown in Fig. 31. Hydrogen will be provided from the outside gas barracks and guided through the existing piping towards the beam line. New gas pipes will be installed along the beam line towards the target area and the TPC location. The gas system itself will be operated by the PLC provided in 2021 by EP-DT.

The goal of the preparations are to have the IKAR TPC operational this year at a maximum pressure of 8 bar and test it with the muon beam of intensities up to 10^7 muons per second. Using an additional gas purification system, the impurities (O_2 and H_2O) can be lower than 1 ppm. The absolute calibration of the pre-amplifiers is required of all channels. An electronic noise level of below 40 keV is expected similar to 2021, allowing a low-energy recoil proton measurement.

5.1.2 Preparation of the New TPC

For the construction of the new TPC an agreement between GSI, TUM, University of Bonn and University of Main was made. This new TPC can later be used at AMBER/CERN as well as FAIR for cross-check measurements, calibrations and other experiments. Due to increasing costs the initially proposed four-cell version of the TPC, adaptions were made to design a modular version of the TPC and reduce the total size to two cells with a possible later extension to four cells. After a world-wide tendering of a company from Denmark is finally contracted. The new version of the TPC has similar properties as the initial one. The anodes will have a diameter of 600 mm covering larger range of protons. A total drift length per cell is 400 mm. Operational pressure will be increased twice allowing twice larger statistics during the experiment as in case of IKAR TPC. In Fig. 32 a 3D model of the new TPC is shown.

The design is verified by the company. The finite element method (FEM) calculations of the deformations and a strength of the elements are performed and a description of the construction process will follow. Furthermore, a CE-certificate will be provided after a successful over pressure test up to 32 bar.

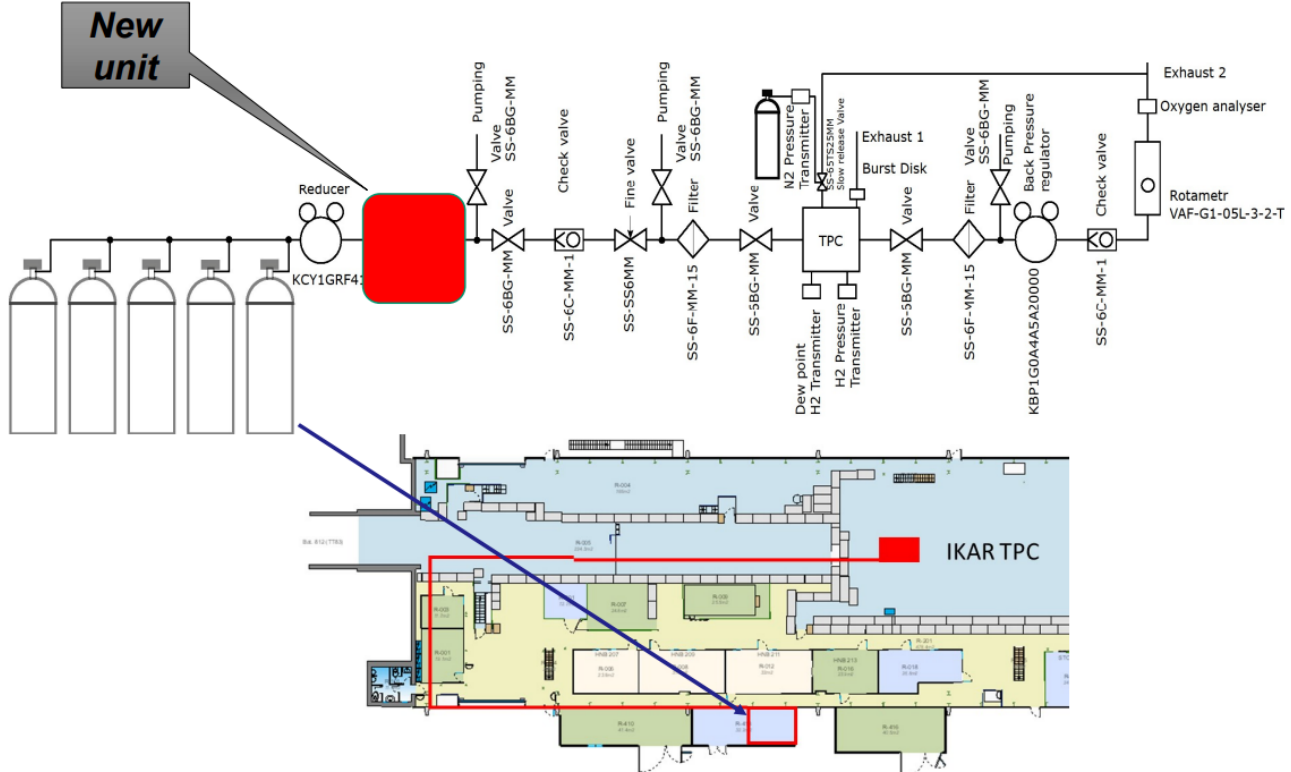


Fig. 31: Sketch of the foreseen IKAR gas system and installation in EHN2. The gas lines are indicated in red together with the new purification unit.

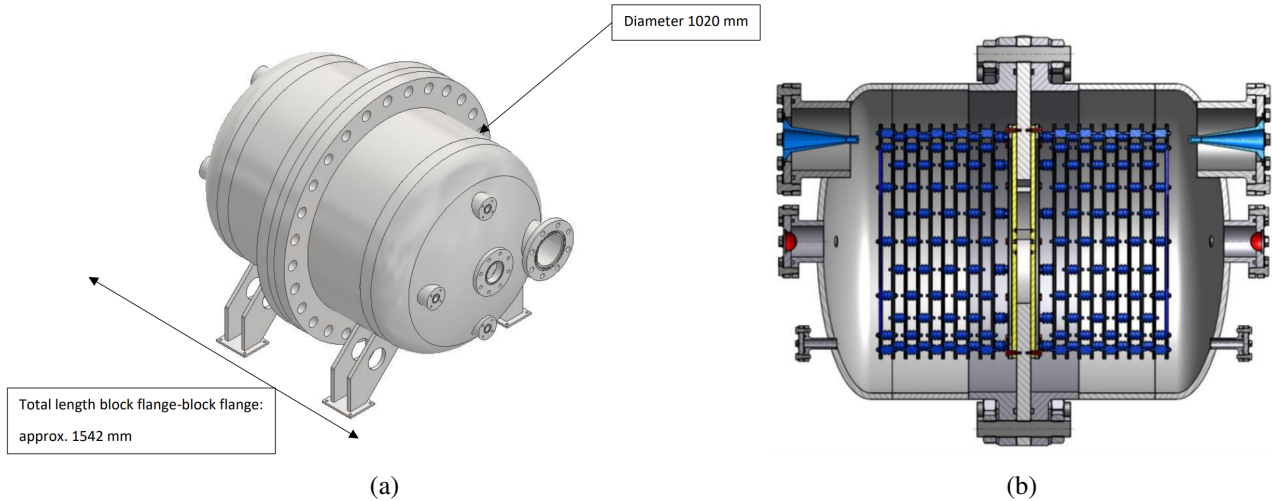


Fig. 32: In (a) a 3D model of the new extendable 2-cell version of the TPC is shown with a sketch of the inner electrodes shown in (b).

The new TPC will use carbon-fiber-based windows instead of Be-windows. Simulations and pressure tests up to 100 bar have been performed. Furthermore, a sample of a new high-voltage feed-through have been tested to withstand pressures of up to 32 bar demonstrating possible usage of the devices for the new detector. For the new TPC, all anodes are read out independently using VME FADC (SIS 3316). A new firmware and readout software was designed and allows higher data rates as well as compatibility of the triggered and streaming (non-triggered) readout.

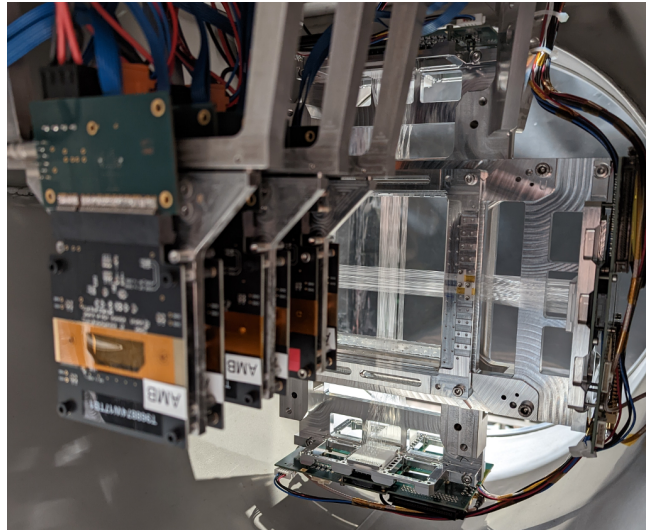


Fig. 33: Inner view of the UTS vessel during the 2022 beam test with six single ALPIDE chips (front) and SFH prototype (back).

5.2 Unified Tracking Station

As described in more detail in the previous report [1], the scattered muon trajectories and the muon scattering angle for PRM is measured by the target tracking system consisting out of four Unified Tracking Stations (UTS). This system consists of Silicon-Pixel Detectors (SPD) based on the ALPIDE monolithic active-pixel sensors (MAPS) and Scintillating-Fiber Hodoscopes (SFH). Developments on both systems are progressing and converging towards a possible application in the PRM physics program. The recent results are presented in the following.

5.2.1 Beam Test in 2022/2023

In October 2022, a beam test of the UTS detector components, was performed in a partially parasitic, partially dedicated manner during the COMPASS and AMBER antiproton production cross-section measurements. For the beam test, prototypes of the respective detector systems were installed. The SPD system consisted out of 6 single ALPIDE chips ($30 \times 15 \text{ mm}^2$) and the SFH was equipped with 4 planes, each with 32 fibers partially readout out on both sides and partially mirrored to study an enhancement of the light yield. An inside view of the mounted detectors is shown in Fig. 33. The main goals of the beam tests were to install the system close to the final location in the target area providing a focused beam, to study the light output of the fibers and the operation of the ALPIDE chips to verify the required tracking capability and efficiencies.

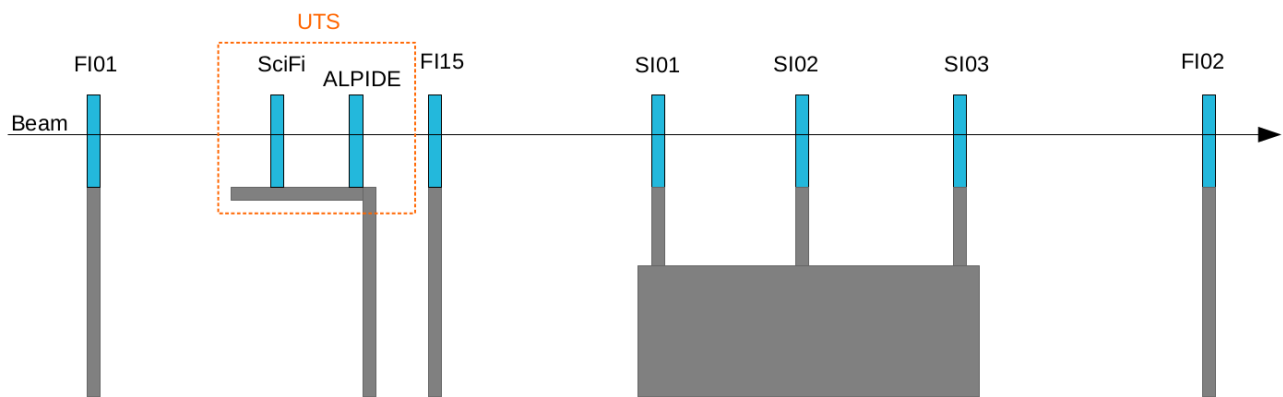


Fig. 34: Sketch of the 2022 UTS beam test setup placed in the beam telescope of the spectrometer.

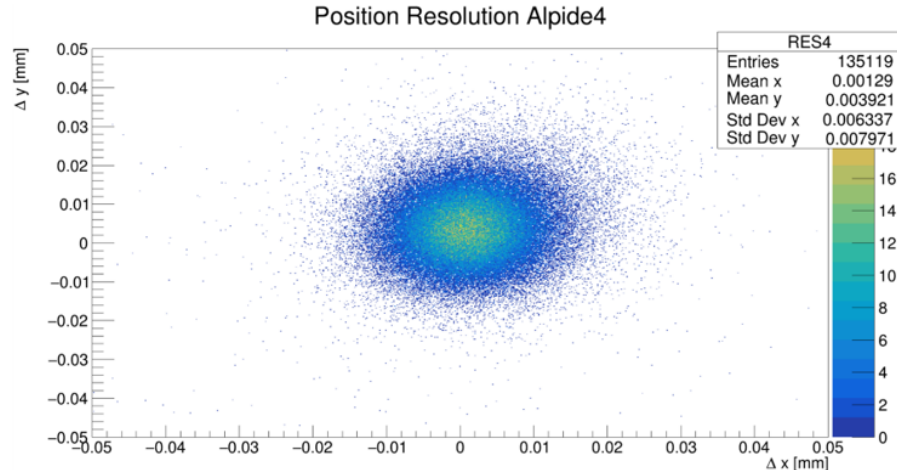


Fig. 35: Position resolution of one ALPIDE detector using tracks measured by the other 5 detectors.

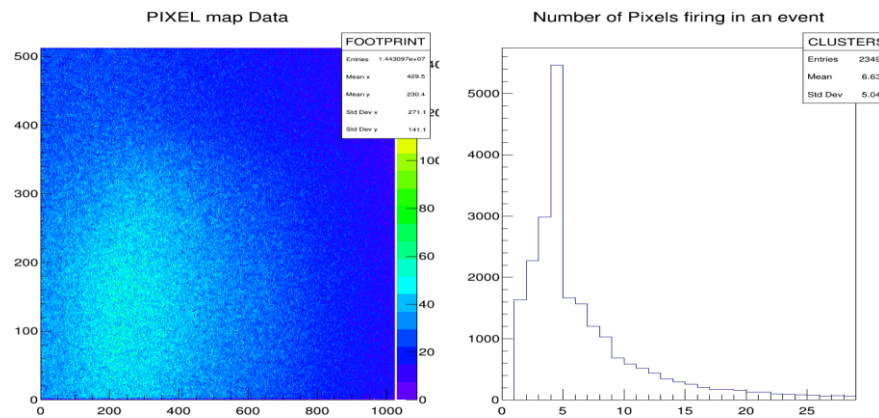


Fig. 36: Left: Beam profile on single ALPIDE chip. Right: Cluster size distribution in ALPIDE detector.

The UTS was installed upstream of the spectrometer target within the beam telescope as shown in Fig. 34, which provided the reference tracking for the studies. During the test, different beam intensities, different ALPIDE settings and various bias voltages for the SFH have been tested. The results are presented in the following.

For the SFH, the readout was based on the so-called MSADC system, which is compatible with the triggered COMPASS DAQ. This allowed a combined data taking of the SFH and the surrounding COMPASS tracking detectors of the beam telescope to evaluate the detector performance as well as the analysis of the spectral response. The SPD used a dedicated DAQ system to study different settings of the chips and the respective influence on the efficiency.

For the SPD, the readout was based on the FPGA modules MOSAIC developed within ALICE ITS for testing and commissioning of the staves in the lab. Still, valuable data on detector performance has been obtained and development of a dedicated tracking algorithm for the ALPIDE test telescope started. An example of the position resolution is shown in Fig. 35 and a cluster size distribution in Fig. 36(right). For the ALPIDE detector response especially this cluster size distribution in the muon beam is of interest to tune the simulation. New FPGA board together with the corresponding firmware and software is developed.

During 2023, a parasitic test stand upstream of the beam dump location of the AMBER spectrometer was used to test the single components of the UTS. So far, test have been performed with the SFH to evaluate new production methods for the scintillating fiber mounting and gluing. The results are discussed in the respective sections.

5.2.2 Scintillating Fiber Hodoscope (SFH)

The SFH consists out of four dense layers of single squared 500 μm thick fibers, individually read out on both ends with SiPMs. A crucial point is the alignment of individual fibers within the active area of the detector. This was evaluated with data from the 2022 beam test. The fibers are grouped in bunches of eight to compensate for variations in the single fiber thickness. In Fig. 37(a) the expected track position for each fiber channel of the X1 plane is shown based on data of the 2022 beam test. Clear shifts and jumps between single fibers are visible. Due to problems with the fixation of the fibers, they were bent inside the active area, which explains the large deviations shown in Fig. 38(a).

Adaptations of the production process were performed to increase the positioning and fixation of fibers for the prototype. These adaptions have been tested during the 2023 parasitic beam test at the test stand upstream of the beam dump of the AMBER spectrometer during the antiproton cross-section measurement. The result of the improved alignment procedure can be seen in Fig. 37(b), where the significantly reduced deviation from the track position is visible. All 32 fibers are centered around zero except for a slight offset, which can be accounted for in the detector alignment procedure. With the improved prototype, the fibers are not bent in the central area anymore, as shown in Fig. 38(b).

An example of the obtained light-yield spectra is given in Fig. 39(a), where only signals with a corresponding track and a correct signal time are considered. The spectrum shows the discrete signal structure of the SiPMs as equidistant peaks corresponding to the number of fired cells. The broad distribution on the right are beam signals, the smaller one the left are dark counts; the two are rather well separated. Fig. 39(c) and Fig. 39(d) show the distributions of mean light yield (in number of fired SiPM cells) for detector configuration used for the 2022 and 2023 prototype tests, respectively. The distributions for both mirrored and unmirrored channels in Fig. 39(c) is quite broad—with the latter being broader—caused by large light-yield variations. To improve the uniformity of the light-yield spectra, the coupling of the fibers to the SiPM arrays was improved for the 2023 test. A new mirroring concept was developed, where the SiPM array can be exchanged with a mirror after production of the detector even during beam time. The resulting distribution, shown in Fig. 39(d), exhibits significantly reduced signal height variations.

Background events at low signal amplitude are dominated by dark counts in the SiPMs. Fig. 39(b) shows the measured total dark count rates for fibers equipped with two SiPMs as a function of the trigger threshold applied (in number of fired cells). The plot nicely demonstrates how the dark count rate can be lowered to negligible levels by requiring a coincidence between the two ends of a fiber. A water-based cooling system is currently in development to reduce and stabilise the temperature of the SiPMs below room temperature, which is expected to further reduce the background rate.

During 2023, the main focus of activities related to the SFH is the production and commissioning of new front-end electronics that are compatible with the new streaming DAQ using the iFTDC. In addition, the design and evaluation of the foreseen cooling system for the SiPMs is pursued and first results are expected towards the end of this year.

5.2.3 Silicon Pixel Detector (SPD)

Position measurement within each UTS will be performed by an array of ALPIDE MAPS sensors. The collaboration has established the necessary licences to hold and operate these sensors at collaboration labs outside CERN for testing and assembly. As outlined in the previous report [1], this sensor can provide an excellent space resolution for the hits relying on $28 \times 29 \mu\text{m}^2$ pixels and providing a spacial resolution of up to $\sigma \approx 5 \mu\text{m}$

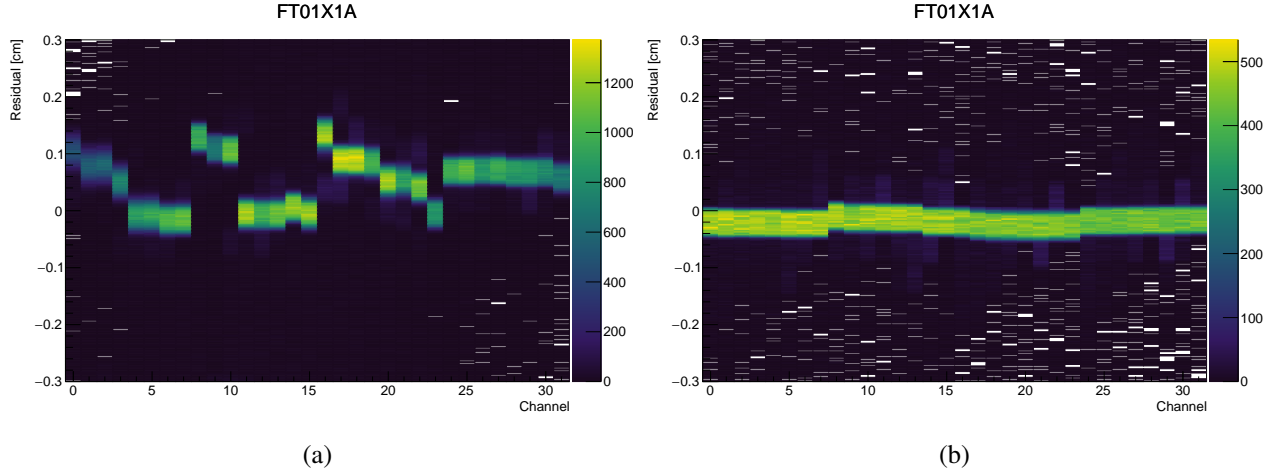


Fig. 37: Panel (a) shows the alignment of individual fibers for the SFH prototype X1A plane during the 2022 beam test, with large fiber-to-fiber variations clearly visible. Panel (b) shows an improved version of the same plane tested in 2023. [11]

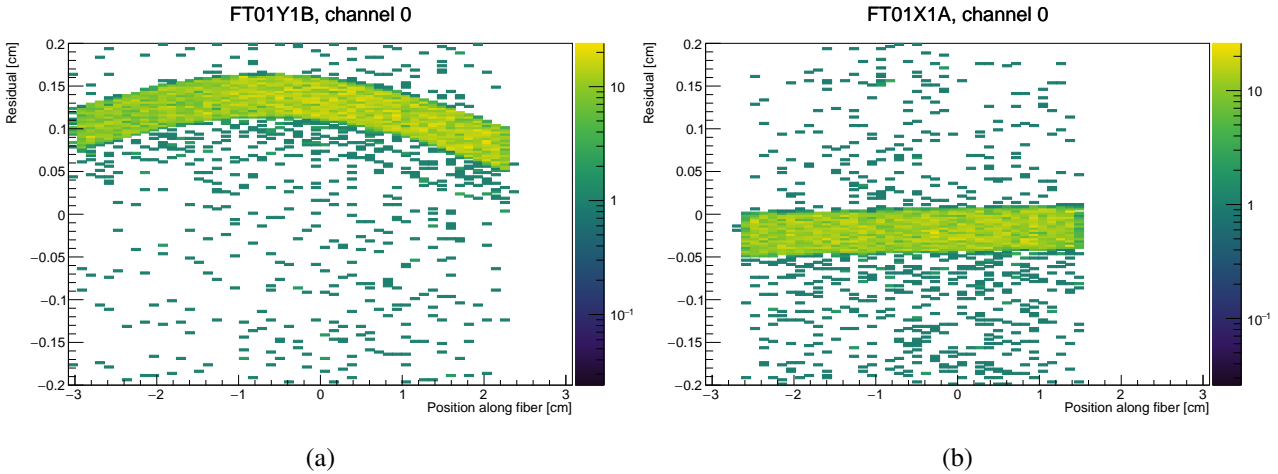


Fig. 38: Using the tracks obtained from surrounding silicon detectors, the difference of the track position and the reconstructed SFH hit position along the fiber was measured during the 2023 beam test. Panel (a) shows an example of one of the planes that were not improved after the test in 2022. Panel (b) shows the improved version of the X1A plane. For both plots, the same cuts were applied on the time and amplitude of the SiPM signals. [11]

for single clusters. To cover the full acceptance, each sensor plane is equipped with 18 ALPIDE sensors, installed in six columns of three sensor each. The ALPIDE sensors are mounted on a custom made flexible PCB back by a thermally conducting Carbon fibre plate for rigidity and cooling. This plate in turn is mounted into an Aluminium frame mounted on a support structure. A Copper cooling pipe inside the Aluminium frame provides heat transport. Transfer PCBs are used to connect the sensors to the DAQ.

The ALPIDE MAPS were developed for the ALICE ITS. While the sensor chip is eminently suitable for the AMBER application, the remainder of the system and the production methods had to be adapted for AMBER including mounting rigs, transport boxes etc. Presently those new elements designed for the assembly of the ALPIDE sensors on the Flex PCBs and then gluing Flex PCBs on the carbon support are tested at INFN Torino and other participating sites shown in Fig. 40. We have already made the initial gluing of the ALPIDE sensors on the Flex PCBs and conducted a further attempt of sensors bonding. Presently the results seem to indicate that the tested part of the new tooling is properly designed with only minor corrections needed. Next steps of the assembly procedure are ongoing and we plan for a first readout attempt of ALPIDEs on Flex PCB. This tooling and Flex PCBs had been designed at INFN Turin and are now transferred to a production site in the UK.

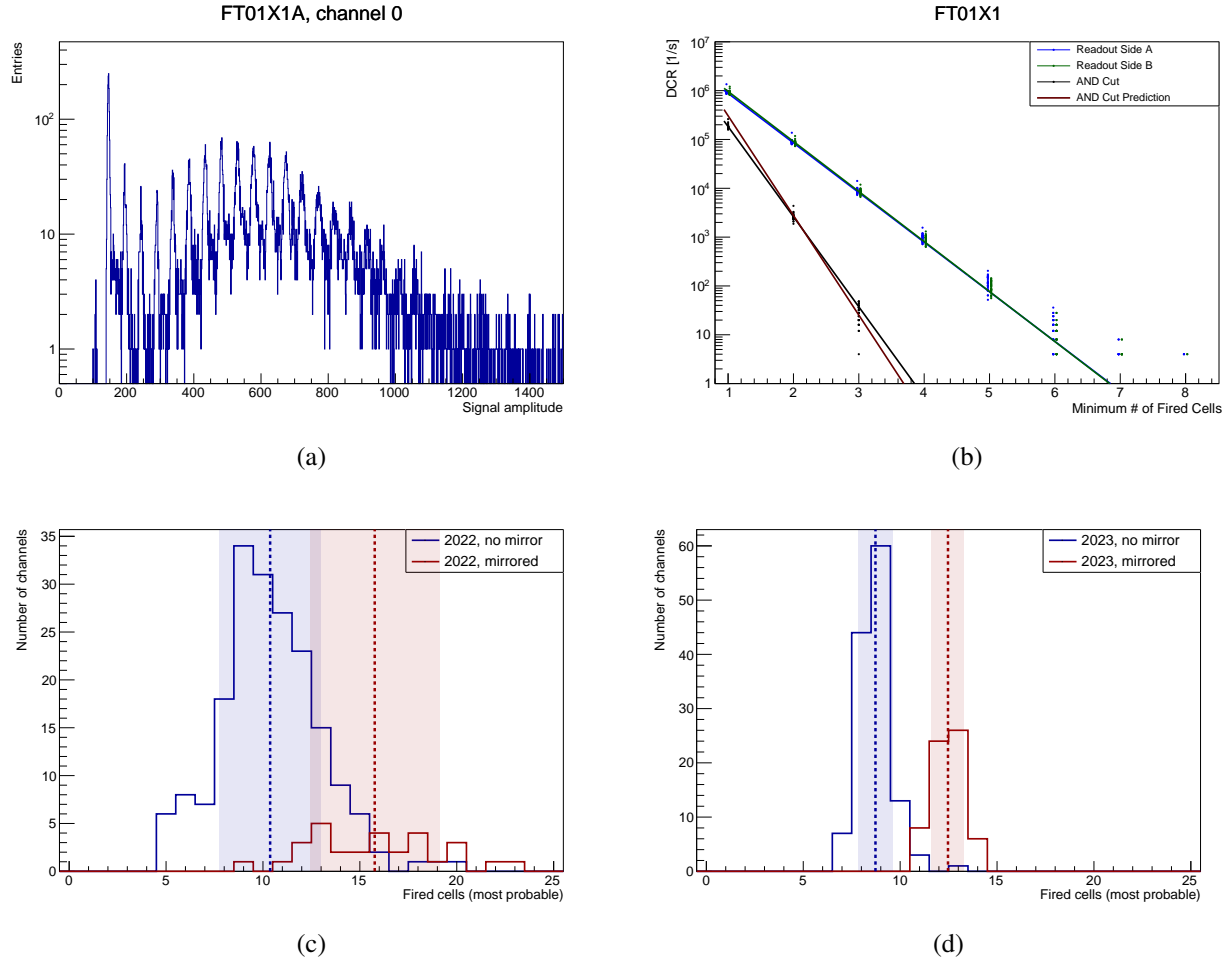


Fig. 39: Characteristics of the SFH signal spectra. Panel (a) shows an exemplary spectrum in a single fiber with one-sided readout (no mirror). Panel (b) shows the dark count rates for single-sided and coincident readout as a function of the trigger threshold (in number of fired cells). Panel (c) shows the distribution of mean signal heights for all fibers of the 2022 prototype test. Panel (d) shows the same distribution for the layers that were improved for the 2023 prototype test. [11]

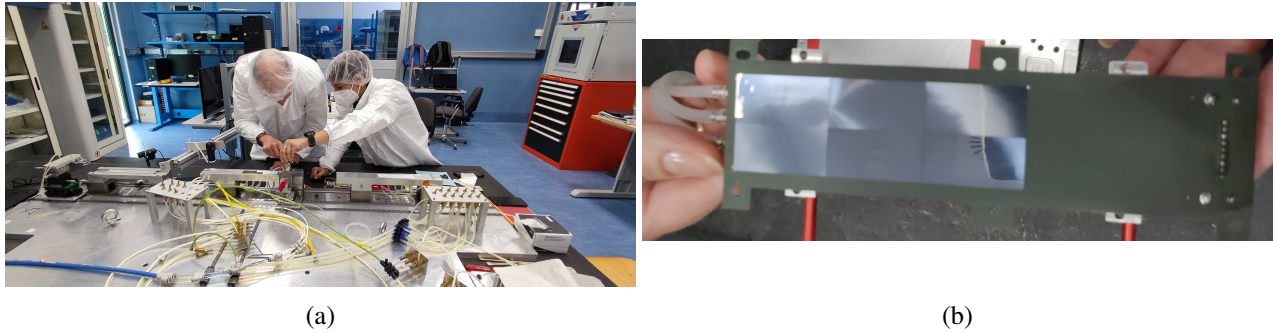


Fig. 40: Photographs of the ALPIDE assembly tests at INFN Turin. In (a) the CMM and assembly rigs used to position the ALPIDE chips on the flex PCBs are shown. The adjacent figure (b) depicts six successfully glued ALPIDE chips on a flex PCB..

The ALPIDE chips are currently being tested and sentenced according to their suitability. Using the ALICE quality standard, out of 414 chips tested, 20.3 % fulfill the *Gold* standard, 31.6 % the *Silver* standard, 7.8 % the *Bronze* standard, with 40.2 % deemed unusable in the experiment, but still useful for practicing the assembly

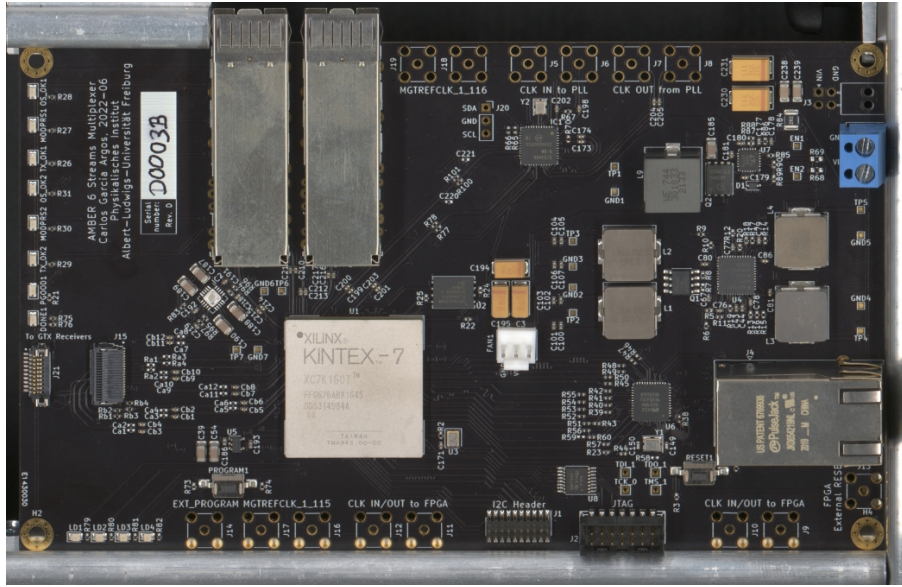


Fig. 41: Prototype of the ALPIDE Detector Specific DAQ Board (CMUX).

and performing mechanical tests.. Note that the actual fraction of usable chips for AMBER might be higher as several features will only be required for the ALICE ITS but not for the AMBER SPD. Evaluation of ALPIDE quality requirements in terms of problematic pixels is foreseen to be performed on simulations using realistic testing results.

Flexible PCBs were designed based on Aluminium tracers to reduce the radiation length of the sensor system. They were ordered from CERN, but suffered from delamination issues causing a delay in the construction of sensor boards for the SPD. Copper plated PCBs were ordered from a commercial supplier to mitigate this shortfall and are being tested. These will be used with low standard MAPS chips to practice assembly and for the prototype test runs despite the moderate increase in radiation length. The delays will result in a reduced configuration for the 2023 test beams, where single sided ALPIDE sensor frames holding 6 MAPS will be complemented by single chip boards as previously used.

The mechanical components have been produced and tested at INFN Turin. Sufficient components for the 2023 beam time are put in production, while alternative production methods simplifying and de-risking the manufacture of the sensor system e.g. through 3D printing of metals, are under study.

ALPIDE Detectors Front-end Electronics The ALPIDE pixel detectors (see Section 5.2.3) feature several readout modes, out of which the one that will be used in AMBER is the high speed serial link, at 1.2 Gbps. The hardware developed at the University of Freiburg for this purpose makes use of a Kintex-7 Xilinx FPGA to read out each group of six chips, taking advantage of the FPGA transceivers that work very efficiently at these data rates and allow for additional tuning of the channels.

The first prototype boards for the ALPIDE data acquisition system were produced in 2021 and have been tested in lab conditions with individual as well as multiple detectors, with no interface to the AMBER DAQ system. The boards include the required connections to communicate with the six ALPIDE detectors, an Ethernet interface for external control, internal clock generation, two optical interface for fast data transmission, and other configurable input/output connections. One of the assembled prototypes is shown in Fig. 41.

The tests performed on the hardware include verification of the signal integrity at the 1.2 Gbps data rate for the ALPIDE detector part, and up to 10 Gbps for the optical transmission and reception side. In addition, the multi-drop busses for the control and clock lines connecting up to six ALPIDE chips was checked.

The firmware implementations include the following features:

- Control of the clock generator to configure the frequencies for the FPGA transceivers.

- Data readout from the transceiver lines coming from the ALPIDE chips, and processing for further transmission.
- Clock generator (40 MHz) and control interface to the ALPIDE chips, for register read/write.
- Data output to SFP+ transceivers, with various protocols: UDP on 10 GbE or UCF on Aurora 8b10b.
- IPBus interface to control the FPGA or the ALPIDE chips, and read out their statuses.
- Debug blocks using Virtual I/O and Integrated Logic Analyser.

The initial development of the firmware lacked direct access to the real chips, which slowed down testing substantially.

Additional supporting hardware for the ALPIDE part of the DAQ has been designed and produced:

- FMC to Firefly and SFP+: an FMC daughter card with two Firefly connectors (one for transmission and another for reception) and one SFP+ cage, that was used for the initial firmware development, by allowing the transmission of synthetic ALPIDE data from a separate commercial FPGA board.
- Telescope Carrier: a card interfacing with ALICE’s single chip carrier cards, for up to 9 ALPIDE chips using the PCI Express connector.
- TCS Receiver: a card featuring a clock and data recovery chip that allows interfacing with the TCS controller.

Currently integration tests with the AMBER DAQ are ongoing at CERN. The setup consists of the CMUX card, using the aforementioned TCS receiver add-on card, and a single ALPIDE detector. The CMUX interfaces with the TCS controller, the DHMux, and the IPBus network.

5.3 New Large Area Micromegas detectors

The present state of the MultiWire Proportional Chambers (MWPC) of AMBER requires that a new detector to substitute some of the stations is designed and produced for the future running. To that goal INFN Torino group is carrying a design study that comprise both a possible new MICRO-MEsh GAS detector (MM) based detector and the corresponding new FEs to fulfill both the detector and the future trigger less DAQ requirements. The design already went through some prototyping steps reaching in 2023 the milestone of the start of the design of a full size prototype together with an active design of a new ASIC. Presently main the requirements for the future detector are derived from the existing performances of the AMBER MWPCs.

Main parameters of the future detector:

- Size: $130 \times 100 \text{ cm}^2$;
- Rates per channel: $< 500 \text{ MHz/strip}$ (passivated center);
- Spatial resolution: 600 μm ;
- Time resolution: 1 ns.

Taking into account that the MM anode and drift electrode will be based on PCBs and that the current PCB production possibilities are limited in size we decided the following configuration for the detector see Fig. 42.

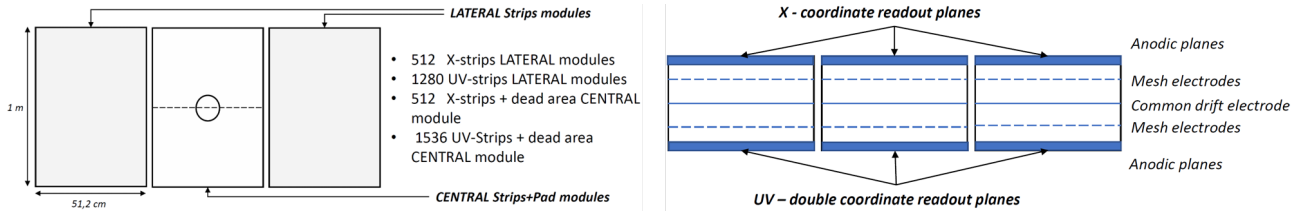


Fig. 42: A frontal and top view of the MM concept that is presently undergoing the design phase

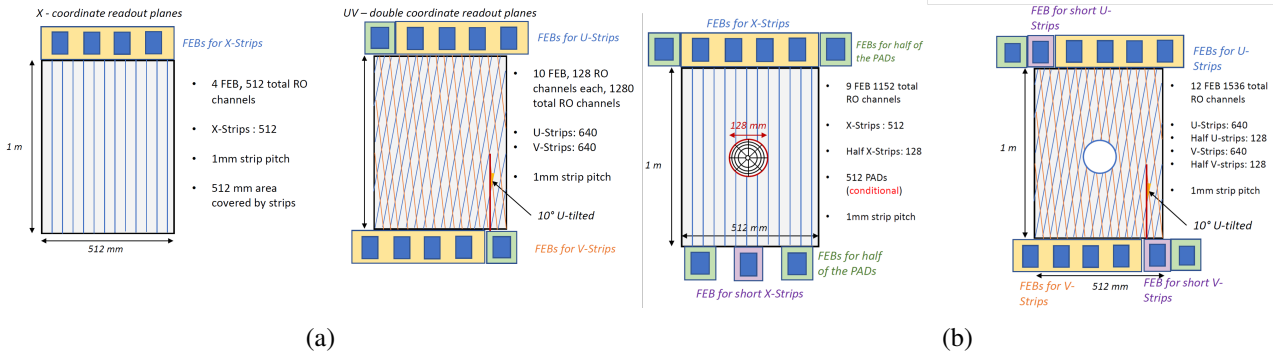


Fig. 43: RO electrodes conceptual configuration. In (a) the lateral module configuration is presented. On the figure (b) the central element is presented.

We can see that the detector is based on individual active areas that form a common instrumented surface of $130 \times 100 \text{ cm}^2$ similar to the present MWPCs. On the Fig. 43, we can see the proposed layout of the strips for the lateral and central modules. Together with the preparation of the detector the work on the test of the small prototypes and design of the DAQ is continued. Presently we use the TIGER (Torino Integrated Gem Electronics for Readout) ASIC in all our ongoing activities as it mostly satisfy the requirements of the MM detector. Instead for the final running within the AMBER program we have started the design of a new ASIC that will be based on the ToAST architecture developed in Torino. The main change that we need to introduce in the new design is the compatibility with the full charge range expected from the MM, the support of higher per channel rates to cope with the events flux in the central part of the detector and on top of that as we need a new ASIC for the MWPC chambers we are integrating the compatibility to that type of detectors. We plan to design a relatively flexible ASIC that could be implemented on more detector systems within the AMBER experiment.

We plan to conclude within the 2023 both the designs of the first full size lateral detector module and of the prototype ASIC.

5.4 DAQ

For the upcoming measurements, AMBER developed a new streaming data acquisition system. A brief description can be found in the previous SPSC report [1]. The streaming architecture takes advantage of modern technology, which allows acquiring, transmitting and processing big amount of data with a small extra cost. This architecture is simple and very flexible as it does not require additional trigger system and dedicated trigger detectors, instead, data reduction is performed by filtering algorithms (HLT) running on conventional computer farm using information from any detector or combination of detectors. In addition, the streaming DAQ is capable merging data of fast and very slow detectors such as TPC with a drift time of $100 \mu\text{s}$. Instead of events the data are organised in time slices of 1-2 ms length. The front-end electronics detects signals and marks them with timestamps referencing timing of signals to the start of the time slice. For some detectors, such as the ECAL, a complex signal shape analysis is performed on the front-end board in order to extract signal amplitude and timing. Afterwards few stages of the FPGA-based hardware merge the time slices from all detectors in one data block and forwards this block to one of Read-Out Engine (ROE) computer in a round-robin manner. This data block includes complete information from all detectors for corresponding time interval. At the next DAQ stage the data are written to a local disk storage providing buffering for up to 3 days of data taking. Then the

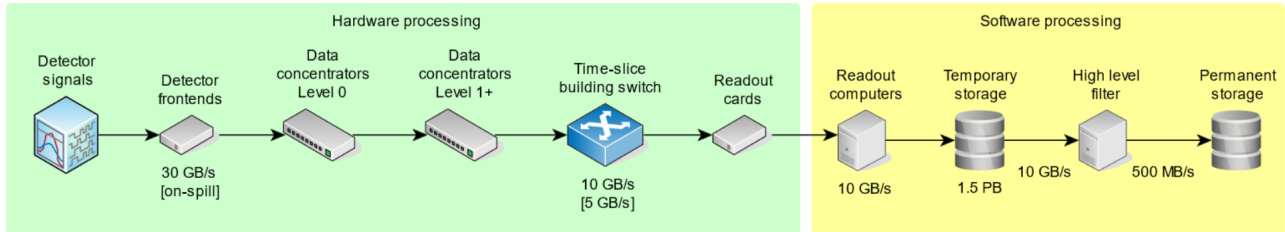


Fig. 44: AMBER streaming DAQ data flow.

data are transmitted to CERN data center via 100 Gbit dedicated network where the HLT algorithms filter them out reducing the amount of data by a factor one hundred. The remained data are forwarded to the CERN Tape Archive (CTA) for a long storage. The sketch of the AMBER streaming DAQ is depicted in Fig. 44.

5.4.1 HLT Structure

The AMBER readout system has scalable architecture optimised for maximal throughput. It can process up to 1 GB/s of data per readout node. For the PRM run we plan to deploy 8 readout nodes. Such amount of data is considerable to store and mostly contains uninteresting information that would normally be filtered out by the trigger system. In the AMBER acquisition system, unwanted data is removed by the high-level filter (also known as HLT). The HLT is a distributed computational framework that is detached from the online DAQ system by a huge local disk storage. Similarly to the main readout system, the HLT is optimised for an arbitrary number of host computers and CPU cores. The system automatically utilises all available resources and distributes time slices to all threads. Thanks to the independent nature of slices, they are analysed on many processors in parallel.

At first, data are transmitted from the local storage to filtering nodes using the RDMA (remote DMA) interface that provides fast data transfers between computers. Then, raw data files are read, and individual time slices are identified within the raw data stream. Each slice is parsed to the level of images, and its object representation is built in memory. In addition, images produced by trigger detectors are decoded in order to extract trigger information from their data words. Such information comes in various forms (e.g., hit times, positions, amplitudes, etc.), and it is forwarded to a filter pipeline for further processing. At the same time, remaining images are kept in the buffers and wait for the final image filtering. The filter pipeline consists of two main stages:

1. **time analysis** (pre-processing) – hit times are taken into account. Timing algorithms search for hit clusters describing particle interactions (event candidates) in the time domain. Meantime is calculated for each cluster and sent to the next stage for spatial validation.
2. **spatial analysis** (filtering) – hit positions are considered. Individual event candidates are examined, and the topology of associated hits is evaluated. If the topology meets the conditions defined in the filter algorithm, the event candidate is marked as valid, and all time-correlated images are tagged for saving. For each event candidate, we always mark two consecutive images to avoid edge cases and loss of information.

Finally, all marked images are written to the output file alongside the list of valid event candidates. While all other images are dropped. Thus, the final amount of data is reduced without changing the data structure. The efficiency of data reduction depends on the selected algorithm and its parameters.

5.4.2 HLT Infrastructure @ Batch Service

After few years of discussions with the CERN network group and beam department we came to a solution which provides a dedicated 100 Gbps network link between the experimental area in 888 and the CERN data center. Actually, two 100 Gbps links have been installed where the second link required for redundancy. The network infrastructure will be completed and commissioned in August 2023. The high speed link provides sufficient bandwidth to transmit unfiltered data to the CERN data center and allows us to operate the HLT

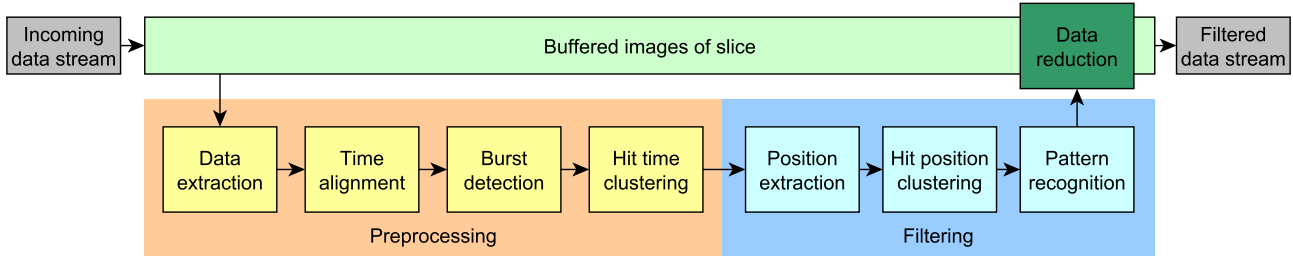


Fig. 45: Filtering pipeline representing a single filtering thread.

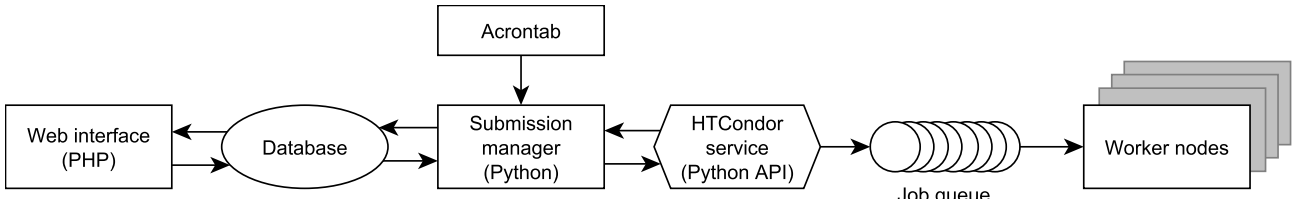


Fig. 46: Architecture of the HLT system running on the Batch service.

framework on shared batch service. In 2022 we discussed with the IT department a possibility to deploy the HLT in the data center and received full support. The HLT framework will run on batch system and may use up to 1000 CPU cores during physics run. Usage of batch system provides a long term scalable solution. It also reduces significantly our needs for local computing infrastructure as well as its maintenance.

In 2023 we tested successfully the HLT framework on a batch system. During the test the data were manually transmitted from the experimental area to the batch farm, processed and then stored on CTA. The data processing chain will be fully automated and tested during this year pilot run. At the moment it allows to collect data with reduced setup and maximum sustained data rate of 1 GB/s.

5.4.3 DAQ Architecture for 2023 Run

For 2023 pilot run we are preparing a reduced DAQ setup depicted in Fig. 47. It consists of six DHMUX FPGA modules, Time Slice builder and two readout engine computers equipped with 480 TBytes of local disc storage. There are also two CMUX FPGA cards connected directly to the time slice builder. The CMUX cards are front-end modules developed for ALPIDE detectors. In the final configuration there will be installed an additional layer of Level One DHMUX modules to support more detectors and utilise efficiently serial links. Right now the system allows to read detectors equipped with iFTDC cards, silicon pixel ASICs, and TPC readout.

The iFTDC is a unified front-end electronics developed for COMPASS and AMBER experiment. It's based on low cost FPGAs and supports scintillation and gas drift detectors. During the pilot run two SciFi and three MWPC stations will be equipped with iFTDCs.

The TPC detector is readout by commercial SIS flash ADC modules. The ADC modules do not support streaming readout therefore we plan to operate them in a self-triggering mode. The trigger is generated when one of ADC channels detects signal above threshold. It's usually initiated by recoil proton while MIP particles produce signals below the threshold. The trigger rate of 100 Hz with 100 μ s detector drift time will introduce 1 % dead time for the acquisition system. The TPC trigger is recorded in one of the iFTDC channels and will be used by HLT for data reduction during PRM physics run. For this year run we installed a new synchronisation scheme between the TPC readout and the acquisition. The AMBER Time Control System provides 19.44 MHz system clock and start of spill signal. These signals are used to generate a time stamp within the ADC modules which can be easily referenced to time stamps of the other detectors. The recoil proton trigger signal is synchronised with time slices and transmitted back to the ADC. The ADC data are collected by a dedicated TPC server and recorder in a separate files. Merging of the TPC data with the rest of the spectrometer is performed by the HLT framework.

There are few objections of this year run:

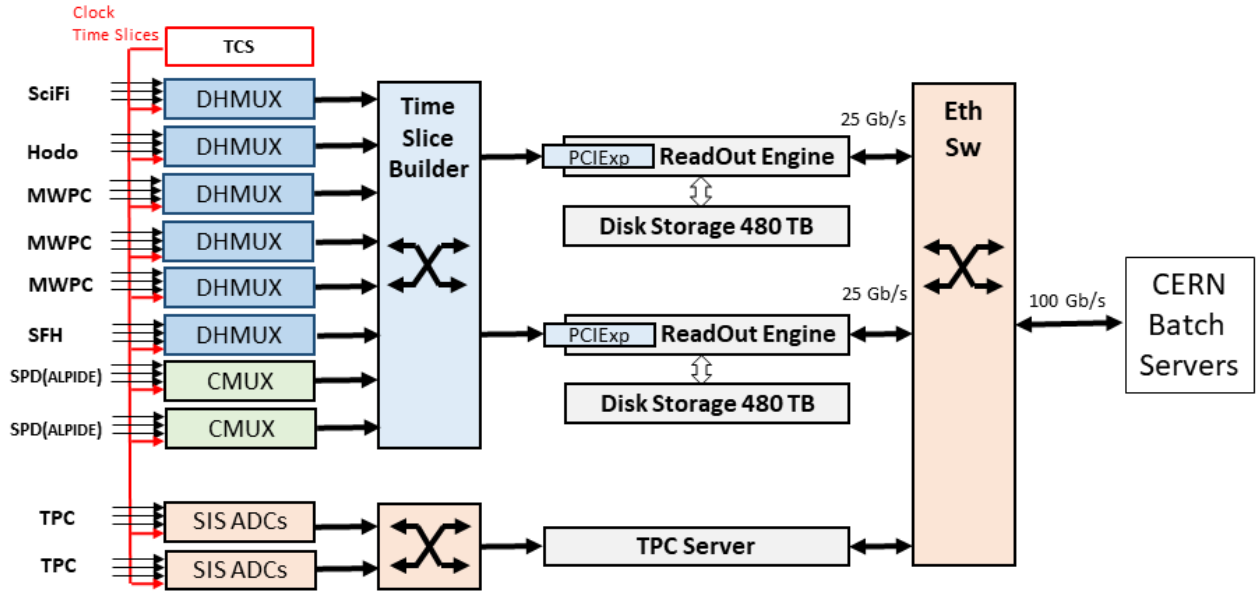


Fig. 47: DAQ overview for 2023 pilot run.

- validation of data flow with real detectors from front-end electronics up to HLT and CTA;
- verification of time synchronisation between detectors;
- verification of real amount of data generated by detectors in streaming mode with the expected one;
- collect data for offline verification and commissioning of fine time synchronisation algorithm.

6 Publications, presentations to conferences and collaboration matters

In the past year, the AMBER Collaboration continued on establishing a protocol for managing its public dissemination and presentation endeavors. This was done by Publication Committee (PubCom), charged with responsibilities of orchestrating and overseeing the internal endorsement process for all AMBER publications, as well as managing the acquisition, distribution, and assignment of talks and presentations throughout the scientific collaboration.

The central objective of the PubCom is to uphold the utmost standards for the public release of various types of AMBER results, encompassing oral presentations, posters, conference proceedings, electronic archives, and journal articles. The AMBER PubCom comprises four members, serving terms of two years. These members are strategically selected to encompass the entirety of the collaboration's scientific endeavors, including the second phase of the experiment. During 2023 a formation of AMBER PubCom has been completed.

During its initial phase, the PubCom is directing its efforts towards contributions to conferences, representing the AMBER Collaboration in the absence of new scientific findings. Serving as a liaison, the PubCom offers a singular point of contact for conference organisers partnering with AMBER. This ensures AMBER's active visibility within the physics community, manifested through prominent participation in pertinent conferences, workshops, and educational events. Regular updates on upcoming conferences are managed by the PubCom and internally publicised within the collaboration. Additionally, the PubCom operates transparently, guaranteeing equitable distribution of presentations among AMBER collaborators, and extends editorial assistance for proceedings conducted on AMBER's behalf.

To maintain uniformity and exceptional quality in contributions made for AMBER, a coherent set of regulations and guidelines has been devised. The adherence to these guidelines is verified through practice sessions conducted within the collaboration. As we progress, these rehearsals are slated to become obligatory. Importantly, these sessions also offer collaborators the opportunity to familiarise themselves with the extensive scientific program of the AMBER experiment, yielding an extra advantage.

The Publication Committee (PubCom) is currently engaged in formulating a set of regulations to govern the approval process for AMBER's physics results. Simultaneously, the PubCom is dedicated to enhancing the content on the official AMBER webpage, ensuring its alignment with the committee's responsibilities and objectives.

Regarding the handling of affiliation information for physicists associated with Russian institutes and the Joint Institute of Nuclear Research (JINR, Dubna), the AMBER Collaboration Board (CB) has deliberated on this matter. In alignment with the policy adopted by major LHC experiments, the CB has chosen to implement a similar approach for AMBER. This policy dictates that authors linked with Russian or Belarussian institutes, as well as those affiliated with JINR, will affix their names and ORCID identifiers (if available) when signing the Collaboration's scientific publications. The institutional affiliation, in turn, will be replaced by the following notation: "Affiliated with an institute [or an international laboratory] covered by a cooperation agreement with CERN." It is important to note that the comprehensive list of authors along with their respective affiliations will be shared with journals in a format suitable for machine-readable analysis or historical reference, albeit not for public display. Notably, the acknowledgment of support from Russian and Belarussian funding agencies and JINR will not be included. However, should the need arise, the experiment management will be prepared to furnish certificates validating the contributions made by the aforementioned institutes, funding agencies, or JINR, to the research presented in the publication.

Additionally, the CB has also reached a resolution pertaining to conference contributions (slides, posters and proceedings) produced on behalf of the AMBER collaboration. This decision specifies that members of AMBER who hold affiliations with Russian institutions or JINR should use only ORCID number as a reference for their institutions, aligning with option established within the framework of the LHC guidelines.

Presentation to Conferences:

- 16 presentations to Conferences and Workshops in a period from May 26th 2022 to August 15th 2023.

7 References

References

- [1] J. M. Friedrich and O. Denisov. AMBER Status Report 2022. Technical report, CERN, Geneva, (2022). URL <https://cds.cern.ch/record/2810822>.
- [2] C. Bovet et al. The CEDAR counters for particle identification in the SPS secondary beams. CERN Yellow Report, CERN 82-13, (1982).
- [3] B. Adams et al. COMPASS++/AMBER: Proposal for Measurements at the M2 beam line of the CERN SPS Phase-1: 2022-2024. Technical report, CERN, Geneva (May, 2019). URL <https://cds.cern.ch/record/2676885>. The collaboration has not yet constituted itself, thus instead of a Spokesperson currently the nominated Contact Person is acting in place.
- [4] Aduszkiewicz et al., Measurements of π^\pm , k^\pm , p and \bar{p} spectra in proton-proton interactions at 20, 31, 40, 80 and 158 GeV/c with the NA61/SHINE spectrometer at the CERN SPS, *The European Physical Journal C* **77** (2017) 671. ISSN 1434-6052. [doi:10.1140/epjc/s10052-017-5260-4]. URL <https://doi.org/10.1140/epjc/s10052-017-5260-4>.
- [5] T. Anticic et al., Inclusive production of protons, anti-protons and neutrons in p+p collisions at 158 GeV/c beam momentum, *The European Physical Journal C* **65** (2009) 9. ISSN 1434-6052. [doi:10.1140/epjc/s10052-009-1172-2]. URL <https://doi.org/10.1140/epjc/s10052-009-1172-2>.
- [6] B. Baatar et al., Inclusive production of protons, anti-protons, neutrons, deuterons and tritons in p+C collisions at 158 GeV/c beam momentum, *arXiv e-prints: arXiv:1207.6520* (2012). URL <https://doi.org/10.48550/arXiv.1207.6520>.
- [7] L. Orusa, M. Di Mauro, F. Donato, and M. Korsmeier, New determination of the production cross section for γ rays in the galaxy, *Phys. Rev. D* **107** (2023) 083031. [doi:10.1103/PhysRevD.107.083031]. URL <https://link.aps.org/doi/10.1103/PhysRevD.107.083031>.
- [8] C. Dreisbach. *Preparations for the Proton-Radius Measurement at AMBER and Operation of Silicon-Microstrip Detectors at COMPASS*. PhD thesis, Technische Universität München, (2022).
- [9] S. Helbing. *Investigation of the Elastic Muon-Electron Scattering in the PRM Pilot Run of AMBER*. Bachelor's thesis, Technische Universität München (Januar, 2023).
- [10] M. Hoffmann. *PhD thesis in preparation*. PhD thesis, University of Bonn, HISKP, (2023).
- [11] K. Eichhorn. *PhD thesis in preparation*. PhD thesis, Technische Universität München, (2023).